Reviewer #1, answers.

We wish to thank the reviewer very much for carefully reading our manuscript and for offering many comments towards its improvement. In revising the manuscript, we have taken into account almost all these comments.

Major comment 1 : It should be clarified which MWR channels are used for each configuration : oblique versus zenith as well as for PR versus NN retrievals. In fact using transparent channels for lower elevation angles is often avoided as the homogeneity assumption is violated (especially if there is cloud or rain in one direction and not in the other direction when the two elevation scans are averaged). Thus, all my interpretation assumed that transparent channels are not used at low elevation angles for the manuscript. If this is not the case and transparent channels have also been used at low elevation angles, the authors should explicit which quality control has been used to identify inhomogenous scenes when they average the two microwave radiometer scans (refer to Cimini et al 2006).

Two identical radiometers (Radiometrics MP-3000A) were used during the XPIA experiment. Both MWRs have 35-channels spanning a range of frequencies, with 21 channels in the lower (22-30 GHz) K-frequency band, from which 8 channels were used during XPIA: 22.234, 22.5, 23.034, 23.834, 25, 26.234, 28 and 30 GHz, and 14 channels in the higher (51-59 GHz) V-frequency band, all used in XPIA: 51.248, 51.76, 52.28, 52.804, 53.336, 53.848, 54.4, 54.94, 55.5, 56.02, 56.66, 57.288, 57.964 and 58.8 GHz, with elevation angles of 90 degrees (zenith) and 15 & 165 degrees (obliques). Section 2.1 has been modified to include these additions.

The Reviewer is correct in assuming that only the opaque channels are used from the oblique scans, when these are used in the Physical Retrieval approach. More specifically, the Physical Retrieval has two options for radiometer measurement inputs: using only the zenith scan, or using the zenith plus oblique averaged scans. From the zenith scan, Tbs from all 22 channels are used in both configurations, while for the oblique scans, when they are included, only the opaque channels (56.66, 57.288, 57.964 and 58.8 GHz) are used. Additional RASS active instrument measurements are used together with the second option, while 2-m in-situ observations of temperature and humidity are used in all configurations. So, Table 1 in manuscript has been revised to be:

	T_{sfc}	Q_{sfc}	Tb_{zenith}	$Tb_{oblique\_avrg}$	$Tv_{RASS915}$	$Tv_{RASS449}$
$\boldsymbol{Y_1}$ = *MWRz*	*X*	*X*	*X*			
$\boldsymbol{Y_2}$ = *MWRzo*	*X*	*X*	*X*	*X*		
$\boldsymbol{Y_3}$ = *MWRzo915*	*X*	*X*	*X*	*X*	*X*	

***Y_4* = MWRzo449**	*X*	*X*	*X*	*X*		*X*

The text has been modified in Section 3.1:

"The MWR provides **Tb** measurements from 22 channels from the zenith scan for the zenith only configuration (**Y_1,** which also includes the 2-m in-situ observations of temperature and humidity), while when using the zenith plus oblique Tb inputs (**Y_2**, **Y_3**, and **Y_4**, also including the 2-m in-situ observations of temperature and humidity) the same 22 channels were used from the zenith scan but only the four opaque channels (56.66, 57.288, 57.964 and 58.8 GHz) from the oblique scans."

The second major comment that should be addressed is about the interpretation of figure 5 where the degradation of the temperature profiles with MWRzo below 200m is attributed to biases in the MWR oblique scans. I think it is important to be rigorous there because nowadays many MWRs dedicated to temperature profiling use low elevation angles down to 5.4° to improve temperature retrievals. Thus, all your interpretation in the manuscript of the improvement brought by RASS measurements is sub-optimal if oblique scans cannot be used (at least for your conclusions below 2 km altitude where RASS brings most of the information). First of all, I think this needs to be addressed in the paper and clearly explained and discussed in the conclusion. Secondly, I also found that the hypothesis provided in line 507 that your degraded results below 200 m with MWRzo comes from a bias is not convincing for several reasons :

→ line 207 : you mention that the two MWR units have a very good agreement in the temperature profiles in the overlapping dates both in terms of bias and correlation. Thus, when you conclude later that the MWR unit used in the paper presents a bias in the oblique measurements it means the two units were in fact biased and not well calibrated, which I found surprising (we can imagine a problem in one calibration but for two calibrations it seems that there is a problem in the deployment)

The NN retrieved temperature profiles from the two MWRs indeed have a good agreement with statistically low bias (0.5 K) and high correlation (0.994). While in line 207 we refer to these statistical measures, line 507 refers to the particular case of March 18, 02:00 UTC which is certainly "a worst case scenario" in the XPIA experiment (certainly a difficult one to retrieve accurately from passive instruments because of the many temperature inversions, three in one profile including one at the surface!)

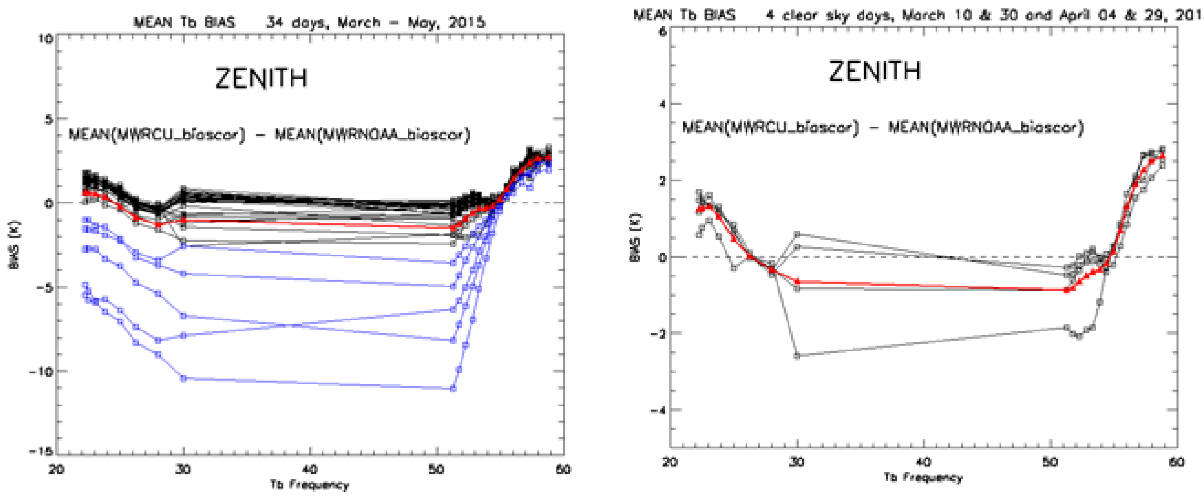

Fig. R1. Difference between bias-corrected Tb of MWR_CU and MWR_NOAA shown for all 34 days when both MWRs were available (left panel) and for the chosen four clear-sky days only (right panel). The averaged difference is shown in red. Blue lines Tb differences correspond to the rainy days.

Previously, in Bianco et al., 2017: "we compared the brightness temperatures (Tb) of the two MWRs for each retrieved channel **for 1 day**, finding almost all channels in good agreement (with differences of ~ 2 K for channels 51.248, 51.760, 52.280, 56.020, 57.288, 57.964, and 58.800 GHz; differences of ~ 1 K for channels 22.500, 26.234, 30.000, 52.804, 53.848, and 56.660 GHz; while the remaining channels did not show appreciable differences)". Using **all available data** from both radiometers we still found that the differences of their daily averaged Tb from the zenith scans, even bias-corrected, were 2-2.5 K for the opaque channels.

→ biases are in general very low for opaque channels that are the most informative below 1 km altitude (and even more below 200m where the degradation is observed). Liquid nitrogen calibration does not change so much the calibration for these channels as they are in general well calibrated by the hot load calibration (every 5 minutes but I do not know if this is the case for the Radiometrics).

Yes, the opaque channels have been changed less than the transparent ones by applying the bias-correction, so the initial difference between the two radiometers for these channels almost did not change. Additionally, the MWR_NOAA Tb had a problem with measurements in the 57.288 GHz channel (with an initial ~ 5 K difference with the MWR_CU Tb) but that difference was reduced in half with the bias-correction.

The Tb difference between the CU and NOAA radiometers for all available dates (34 days) after applying the bias-correction for the opaque channels (>56.5 GHz) still shows a difference around 2-2.5 K, while for the transparent channels (52-56 GHz) the differences are mostly improved with the final biases < 1.5 K. Finally, the K-band channel biases were not extremely large even without bias-correction, and after bias-correction they are less than a degree K different.

→ In figure 6, we can also see that NN retrievals using oblique measurements manage to improve NN with zenith only below 700 m, the degradation appears above 1 km when transparent channels are used and are more subject to large biases. Thus, the use of opaque channels below 700 m does not seem to degrade NN retrievals as much as shown for PR below 200m in figure 5. We observe the same thing in figure 2 : if we look at the NN retrievals, there is a significant modification of the profile below 250m when including oblique measurements that we do not observe with the physical retrievals.

In order to confirm your hypothesis, could you check the biases for oblique measurements as it is done in figure 1 ? If you compared to simulated TB from radiosondes and assuming homogeneity in an area around ~ 1km from the instrument, could you re-use the RS to investigate more in depth the biases at low elevation angles (as it is done in figure 1) to confirm this hypothesis ? Alternatively, you could also use model data (analysis or very short-term forecasts) during clear-sky conditions similarly to the paper of De Angelis et al 2017. I think this check is very important to confirm your conclusions lines 507 and 521. Depending on your answer about the channels used at oblique measurements, did you try to restrict MWRzo to only the most opaque channels (very close to 58 GHz)? It would be interesting to identify if the supposed bias occurs for all V-band channels and/or only the most transparent ones

Following the reviewer's suggestion, we compared the Tb measurements from the opaque channels for the same time shown in Fig.5 of the manuscript with Tb calculated by the forward model applied on the radiosonde data, Fig.R2 below:

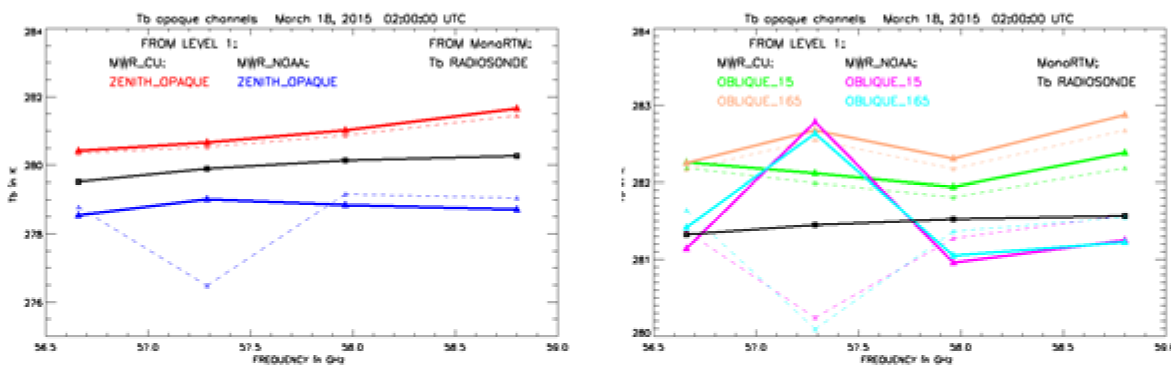

Fig.R2. March 18, 2015, 02:00 UTC: the Tb of the opaque channels, 56.66, 57.288, 57.964 and 58.8 GHz, from the zenith scans (left panel) of the MWR_CU in red and MWR_NOAA in blue and from both oblique scans (right panel) in colors, and the Tb from the MonoRTM forward model using the corresponding radiosonde profile in black. Dashed color lines mark the original Tb data and solid color lines – bias-corrected Tb.

For this time period the bias-correction does not improve the Tb observed by the MWR compared to those derived from the radiosonde, the bias-corrected Tbs are further from the radiosonde Tbs compared to the uncorrected Tbs, except for the 57.288 GHz channel of the MWR_NOAA that shows measurement problems before bias correcting it. We have to admit that radiosonde Tb data cannot be claimed as the "true" because these data are the output of the forward model that has its own uncertainty.

The bias-correction in general improves the temperature profiles for most of the test time reducing the bias in the 1-2 km AGL layer by 0.5 K for all PR averaged profiles.

Additional text included in Section 3.2 (with some editing): "We compute the bias in the bias-correction procedure only from the zenith scans assuming that the same bias is suitable for the oblique scans. Also, we use the assumption that the true bias is an offset that is independent of the scene, so that the sensitivity to the scene (e.g., clear or cloudy, zenith or off-zenith) is small. To investigate this we eliminated the radiosondes launched during rainy periods (5 out of 58 cases) and found that the averaged temperature profiles were very little different than when all radiosonde profiles."

Fig.R2 shows the bias between the opaque channels' Tb and radiosonde-derived Tb. While these differences are similar in absolute values, but of opposite sign, for the zenith scans, the oblique channels show a noticeable difference between MWR_CU and MWR_NOAA Tbs compared to radiosonde Tbs (Fig.R2, right). These differences resulted in very different PR profiles from the two radiometers, as shown in Fig. R3:

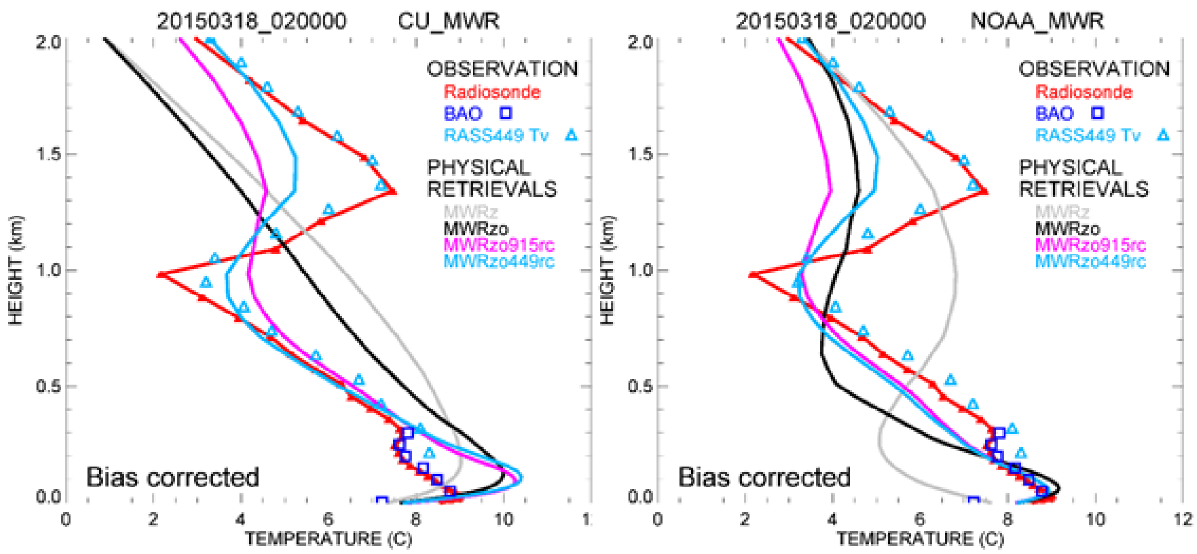

Fig.R3. March 18, 2015, 02:00 UTC case. Observations from radiosonde are in red, and from BAO seven levels – in blue squares. The four PR profiles are in gray (MWRz), black (MWRzo), magenta (MWRzo915) and light-blue (MWRzo449). PRs from the MWR_CU are on the left and from the MWR_NOAA - on the right.

According to the right panel of Fig.R2, the MWR_CU has a bigger Tb bias for the opaque channels from the oblique scans compared to the MWR_NOAA measurements for this case, that resulted in MWR_NOAA temperature profile to be closer to the radiosonde profile in the layer of 0-300 m above the ground, shown in Fig.R3.

Still, with the measurement problem in the 57.288 GHz opaque channel of the MWR_NOAA instrument, and because of its limited time availability during the XPIA campaign, we decided to limit our analysis to the MWR_CU data only.

Second major comment about NN retrievals: Line 347 you mention that you cannot un-bias the BT from neural network. I can understand especially if you did not train the neural network by yourself but I think this is a major concern in all your evaluation of the next sections. We can see that NN retrievals have a degraded accuracy due to an increase bias above 1 km altitude which is probably due to the large V-band bias for transparent channels. However, after this small remark line 347, you never discuss this issue again. I think it is not fair when you compare with the PR which takes into-account a bias-correction which is very large for transparent V-band channels. At minimum, the authors should always remind this limitation to the reader : the problem might not be due to the NN approach itself but to a biascorrection that needs to be applied to NN retrievals similarly to PRs (you should also cite Martinet et al, Tellus, 2015 which shows how NN bias can be decreased after bias correction).

I am also wondering if, through the manufacturer software, you could re-process the NN retrievals by modifying the binary of TB files including the bias that you provided in figure1. This should be feasible and at least would give some ideas if the NNs are improved when using the same BT as for PRs (but keeping in mind that your bias correction for NN would not be perfect as probably a different RTM has been used to deduce the bias and train the NNs).

I also only understood at the end of the paper that the green line for the NN oblique measurements never use zenith observations. Thus, I assume NN with oblique measurements only does not use transparent channels as this would violate the homogeneity assumption. So, it is totally normal that the bias of NN with oblique measurements is degraded above 1 km altitude…If NN with oblique measurements only use opaque channels at low elevation angles, all your results to compare with NN retrievals should combine the two temperature profiles that you obtain: the one from zenith only mainly above 1 km altitude and the one obtain from oblique measurements below 1 km altitude. This has to be done if you want to compare with the configuration MWRzo which uses both zenith and oblique measurements. If I also understood correctly that zenith observations are not used for NN retrievals I think that figure 8 should stop at 1 km above ground maximum and not 5 km. Either you want to go up to 5 km altitude and you need to create a composite temperature profiles from the NN retrievals and make again your statistics with this new profile. Or you should limit your averaging of the bias and RMSE up to 1 km altitude because you cannot take into account statistics from the NN which are biased because they do not use observations informative of higher altitudes (or observations which are not bias corrected like the PRs).

We thank the referee for this particular comment. Following the very insistent recommendation of Reviewer #2 and your questionable opinion about the temperature comparison of bias-corrected input for the PR data and uncorrected NN data, we decided to move all comparisons of PR and NN profiles to Appendix A. The suggestion about NN bias-correction using the Tb biases from PRs looks interesting, but we decided not to mention it because of the artificial mix of two approaches. Instead, we included (in Appendix A) the comparison of PR profiles with separate NN profiles from zenith and from oblique averaged scans and with NN profiles calculated from the combination of the scans using NN oblique scans up to 1 km and NN zenith scans above.

Technical corrections:

Introduction, line 109 : I think the sentence is a bit too long and complex to follow. The radiative transfer equations are in general used to train the neural network retrievals or used directly inside physically-based retrievals whereas from the sentence it seems not connected. I think the sentence would be more rigourous rephrased that way :

« in order to estimate profiles of temperature and humidity from observed brightness temperatures, they apply regressions, neural network retrievals or physical retrieval methodologies which include more information about the atmospheric state in the retrieval process. Radiative transfer equations are commonly used to train statistical retrievals or as forward models inside physical methods».

Rephrased as suggested.

Introduction line 116 : I do not agree with the argument that MWRs have a limited accuracy due to the fact that they do not actively measure temperature and humidity profile. We can of course improve their retrievals but it is hard to find sensors with accuracy better than 0.5 to 1.5 K during all conditions for temperature. I agree with the other drawbacks (lower accuracy during rain, coarse vertical resolution especially) but not with that one or you should give more arguments.

We deleted the comment on the accuracy of temperature and humidity measurements.

Introduction line 121 : site specific climatology is only a disadvantage for regressions or neural networks. This is not the case when using 1D-Var retrievals combined with model outputs. I think it would worth mentioning a few reference papers using 1D-Var approaches combined with NWP model : Hewison 2007, Cimini 2011, Martinet et al 2020 etc..

We have now added the following text in the Introduction, together with the mentioned References: “Some studies have used analyses from NWP models as an additional constraint in these variational retrievals (e.g., Hewison 2007, Cimini 2011, Martinet et al. 2020); however, we have elected not to include model data in this study because we wanted to evaluate the impact of the RASS profiles on the retrievals from a purely observational perspective “

Introduction line 125 : The literature refers more to low accuracy of MWR LWP retrievals forvalues below 20 g/m², 50g/m² seems a bit overestimated please modify or provide a reference for

this statement.

Changed from 50 to 20.

Introduction line 142 : add an « s » to lowest several kms.

Included.

Section 2, line 172 : change included into including.
"Included" is right.

Section 2, line 196 : change manufacturing into manufacturer.
Changed.

Section 2.1, line 203 : Please correct into : « NN zenith and of the NN oblique measurements. »
Included.

Section 2.1, line 205 : can you mention the date of the last calibration with liquid nitrogen for the
data used in the paper ?

Prior to the experiment, both MWRs were calibrated using an external liquid nitrogen target and an internal ambient target and thoroughly serviced (sensor cleaning, radome replacement, etc.). The MWR used in this study was serviced and calibrated on 2/27/2015. This text was included in the manuscript.

Section 2.2, line 221 : can you mention in which conditions RS were launched (how many clear-sky
or cloudy-sky?)

Of 58 valid radiosonde profiles, 41 were launched in clear-sky periods, 12 - in cloudy periods, and 5 during rain. We defined those categories using Tb in the 30 GHz channel, as shown in the figure below:

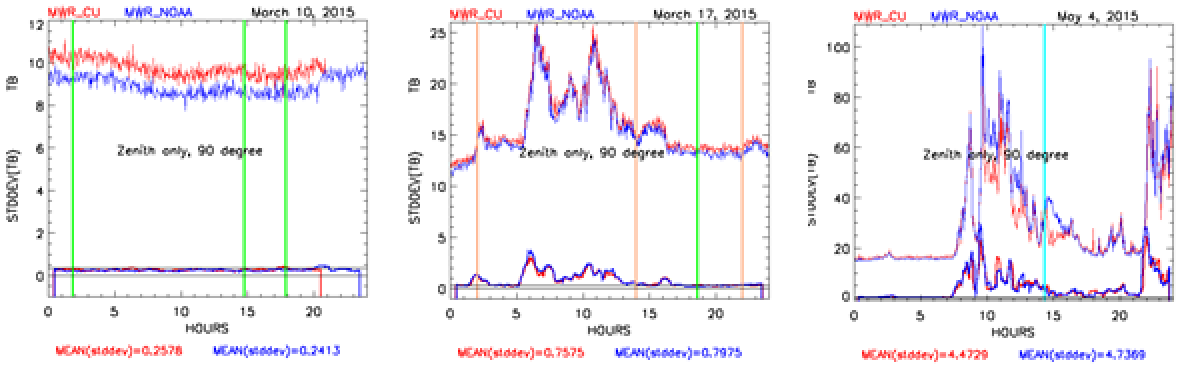

Fig.R4. Zenith Tb from the 30 GHz channel for a clear-sky day (left panel), cloudy day (middle panel) and rainy day (right panel) from the CU radiometer in red and NOAA radiometer in blue. STDDEV(Tb-SMOOTH(tb,11)) is shown at the bottom of each panel with its average values printed under the panels in corresponding colors. Vertical lines (green – for clear-sky, beige – for clouds and cyan – for rain) show the time of radiosonde launches.

We also included the following text in the manuscript:

"Four clear-sky periods have been chosen using a criterion of less than 0.3 K uncertainty in the 30 GHz channel: March 10 and 30, and April 13 and 29, 2015. During periods with liquid-bearing clouds overhead, this criterion is markedly higher (more than 0.7 K) and much higher for the rainy periods (> 4 K). While those calculations were applied on a daily basis, it is important to mention that the days are not uniform in terms of cloudiness or rain. Therefore, we used the data for the 2-3 hours bracketing the time of radiosonde launches to determine to which category a particular radiosonde profile belongs, clear-sky, cloudy or rain. In this way, we found that from 58 radiosonde launches used in our statistical analysis, 41 belong to the clear-sky category, 12 - to cloudy but non-precipitating conditions and 5 - to rainy periods."

Section 2.3, line 225 : Please correct same location as the MWR.
Corrected.

Section 3.1, line 270 : please specify : integrated content of liquid water
Included.

Section 3.1, line 282 : could you add some spaces between the Sa matrice and the specification of
the Jacobian Kij ? Could you also specify in this notation what is i and j ? (I assume channel and
vertical level). Could you be consistent with the definition of Xa line 267 (always use L for LWP or
only LWP everywhere) ?
Xa and Sa are changed (from L to LWP). Jacobian is moved to form the straight-line definition.
Notations of "i" and "j" are included.

Section 3.1, line 294 : can you say a word on how the Sa matrix has been computed ?Section 3.1, line 296 : can you mention the perturbation size that you used to compute your Jacobeans ?
We included the additional description of the Sa matrix in the text in Section 3.1: "Using 3,000 radiosonde launched by the NWS in Denver, we interpolated each profile to the vertical grid used in the retrieval, after which we computed the covariance of temperature and temperature, temperature and humidity, and humidity and humidity for different levels."

Section 3.1, line 300 : could you please mention which MWR channels are used in the retrievals for
zenith only and for oblique measurement ? (all of them or just a sub-sample .).
As mentioned earlier, 22 channels were used from zenith measurement and 4 channels (opaque) – from oblique (included in Section 3.1).

Section 3.1, line 312 : could you mention the uncertainty values used in the Se matrix ?

The uncertainty in the MWR Tb observations was set to the standard deviation from a detrended time-series analysis for each channel during cloud-free periods. The derived uncertainties ranged from 0.3 K to 0.5 K in the 22 to 30 GHz channels, and 0.5 to 1.0 K in the 52 to 60 GHz channels. We assumed that there was no correlated error between the different MWR channels.

For the RASS, collocated RASS and radiosonde profiles were compared and the standard deviation of the differences in Tv were determined as a function of the radar's signal-to-noise ratio (SNR). This relationship resulted in uncertainties that ranged from 0.8 K at high SNR values to 1.5 K at low SNR values. Again, we assumed that there was no correlated error between different RASS heights.

These additions are also included in Section 3.1.

Section 3.1 and table 1 : Does Tbzenith-oblique means both TB measured at zenith and at oblique
elevation angles ? If this is the case, why there is a cross at the column indexed « Tbzenith » too ? It
is a bit confusing as it seems that Tbzenith is used twice in the retrievals which I assume is not the
case. Could you clarify this point in table 1 but also line 283 in the Se matrix ?

Table 1 as well as observational vectors Y2, Y3 and Y4 and matrix Sε have been modified.

Table 1 with its modifications has already been shown above. Vectors Y2, Y3 and Y4 and matrix Sε are modified as follows:

$$\boldsymbol{Y_1} = \begin{bmatrix} T_{sfc} \\ Q_{sfc} \\ \boldsymbol{Tb_{zenith}} \end{bmatrix} \qquad \boldsymbol{Y_2} = \begin{bmatrix} T_{sfc} \\ Q_{sfc} \\ \boldsymbol{Tb_{zenith+oblique\ avrg}} \end{bmatrix}$$

$$\boldsymbol{Y_3} = \begin{bmatrix} T_{sfc} \\ Q_{sfc} \\ \boldsymbol{Tb_{zenith+oblique\ avrg}} \\ \boldsymbol{Tv_{RASS915}} \end{bmatrix} \qquad \boldsymbol{Y_4} = \begin{bmatrix} T_{sfc} \\ Q_{sfc} \\ \boldsymbol{Tb_{zenith+oblique\ avrg}} \\ \boldsymbol{Tv_{RASS449}} \end{bmatrix}$$

$$\boldsymbol{S_\varepsilon} = \begin{bmatrix} \sigma^2_{T\,sfc} & 0 & 0 & 0 \\ 0 & \sigma^2_{Q\,sfc} & 0 & 0 \\ 0 & 0 & \boldsymbol{\sigma^2_{Tb_{zenith}}}\ \text{1}\ \ \boldsymbol{or}\ \boldsymbol{\sigma^2_{Tb_{zenith+oblique\ avrg}}}\ \text{2} & 0 \\ 0 & 0 & 0 & \boldsymbol{\sigma^2_{Tv_{RASS915(449)}}}\ \text{3 or 4} \end{bmatrix}$$

Section 3.1, line 278 : the sentence is confusing. It seems equation (1) is here to show how the Y

vector is estimated from the state vector X whereas equation (1) shows the new atmospheric state

updated at each iteration of the minimization depending on the previous state, the different matrices

(Sa, K, Se) and the forward model. Please correct the sentence accordingly so that it makes more

sense.

Corrected in Section 3.1: "The MonoRTM model **F** is used as the forward model from the current state vector **X**, Eq. (1), and is then compared to the observation vector **Y,** iterating until the difference between **F(X)** and **Y** is small within a specified uncertainty."

Section 3.1, line 313 : please correct the sentence into : « its dimension increases ».

Done.

Section 3.2, line 319 : please correct into « will contribute to a bias in the retrievals ».
Done.

Section 3.2, line 328 : could you mention what thresholds and criteria you used from the 30 GHz Tb

to identify clear-sky periods ? (standard deviation over which time period and which threshold?)

This text was added to Section 3.2 (with some editing):

"A threshold value of 0.3 K has been used for the uncertainty calculation. Fig. R5 (see below) shows one of the clear-sky days, March 10, 2015. The final uncertainty equals the average of the Tb standard deviation in a one-hour window sliding through all data points of a day. It also could be computed as the standard deviation of the difference between Tb and smoothed Tb to eliminate daily temperature variability. Finally, there is a "standard" set of uncertainties used as the high boundaries for Tb uncertainty per MWR channels calculated empirically in previous experiments."

"For the four chosen clear-sky days not only the daily uncertainties of **30 GHz Tb** were below 0.3 K, but all three sets of uncertainties described above were extremely similar with the averaged difference less than 0.05 K."

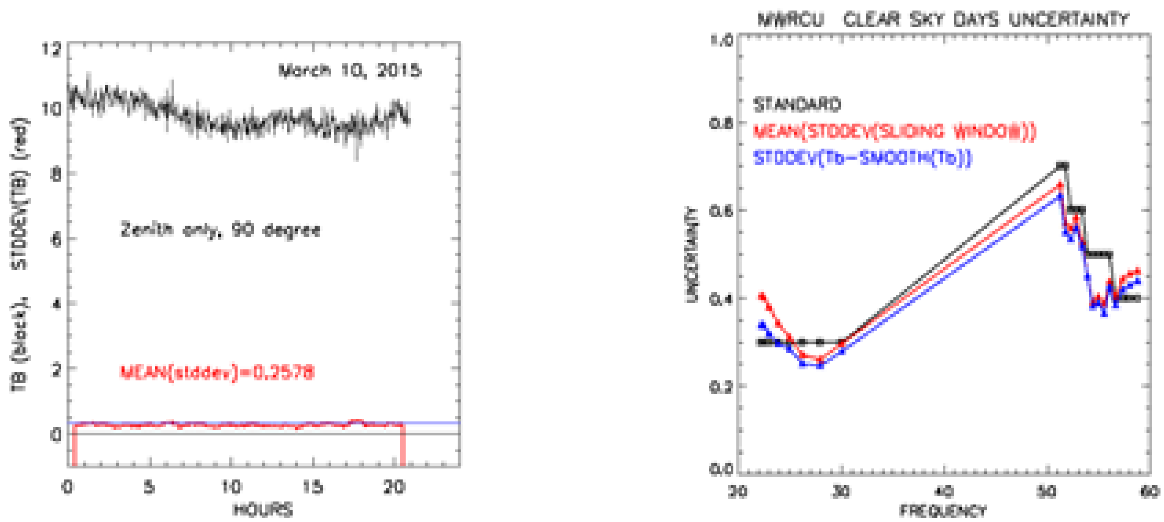

Fig. R5. Left: Tb from MWR_CU 30 GHz channel for March 10, 2015, one of the chosen clear-sky days. The standard deviation (at the bottom, in red) is calculated as the averaged standard deviation of Tb in a one-hour window sliding through all data points of the day. Right: MWR_CU uncertainty, computed as an average over four clear-sky days using a sliding window (in red), smooth function (in blue), and the before mentioned “standard” values (in black) for all 22 channels.

Section 3.2, line 333 : How the bias is computed ? Is it a difference with simulated BT from radiosondes ? Can you please clarify this in the manuscript.

From the modified text in Section 3.2:

“The bias was computed for each of the 22 channels as the averaged difference between the Tb from the MWR zenith observations, and the forward model calculation applied to the prior, over these selected clear-sky days, and then subsequently removed from all of the MWR observations.”

Section 3.2, line 345 : can you at least mention that NN biases could be improved by applying a bias-correction ?.

We moved the NN and PR comparison in Appendix A and mentioned this possibility.

Section 3.2, figure 2 : Can you specify if it is a clear-sky day or a cloudy day ? I suspect that this is a cloudy day with elevated inversion which often causes trouble to MWRs. If possible, a comparison with a clear-sky day by night with a sharp temperature inversion close to the surface could be interesting too. Could you say a word in the manuscript why you are have 0.5 to 1K

difference between the RS measurements and the BAO tower measurements which are used a the
« truth » for validation ?

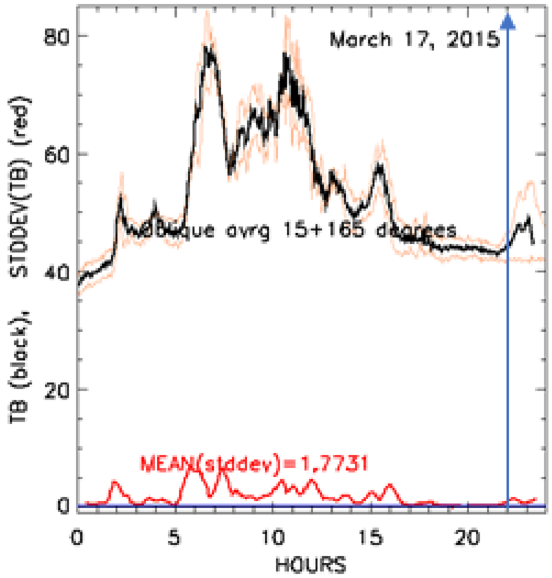

Fig.R6. Oblique channels Tb from 30 GHz channel, March 17, 2015. Blue arrow marks the time of the day, 22:00 UTC, for the radiosonde case shown in Fig. 2 of the manuscript.

This is the 30 GHz channel Tb from the oblique scans. A difference between the two scans of 15 and 165 degrees at 22:00 (time of the radiosonde launch) just started to grow that may indicate the cloudiness in the view of one of the obliques.

Fig. 5 in the manuscript shows exactly one of the difficult cases you are mentioning: evening hours with sharp temperature inversions, one of them close to the surface.

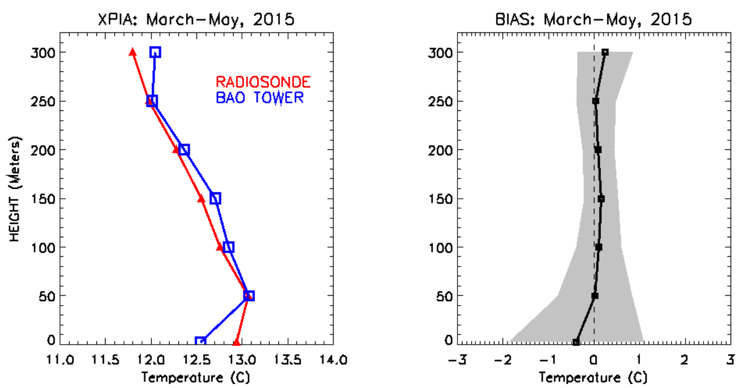

Fig. R7. Averaged temperature at BAO tower heights from radiosonde (red) and from BAO levels (blue) in the left panel and their biases at each level with shaded image of standard deviation over 58 radiosonde launches in the right panel.

We indeed use BAO measurements as the "truth" having very close agreement between the radiosonde and BAO measurements. The special case of Fig. 2 in the manuscript has larger differences between the radiosonde and BAO, which on average were less than 0.5 K, which is within the expected accuracy of the radiosondes.

Section 3.2 line 366 : Modify the sentence into « demonstrate a better agreement ».
In the text now: "the MWRzo449 profile (in light-blue) demonstrates a better agreement"

Section 3.3, line 388 : please rephrase into « Akernal provides useful information ».
Done.

Section 3.3, line 425 : please correct vs into versus.
Included "versus".

Section 3.3, figure 3 : As it is, Panel a) does not sound really relevant to me as it is the same as
figure 2. However, in this section we would expect to see the smoothed RS profiles for the two
configurations selected (MWRzo and MWRzo449). Could it be added to panel a) ?
Can you also explain why you get a strange vertical line in the Atkernel on the left part of the
figure ?
The smoothed Radiosonde profiles from MWRzo and MWRzo449 are included in panel R8a).

First left vertical lines in panels R8b-c) indicate surface data (see the definitions of observational vectors Y). To confirm this, we repeated those runs without including surface temperature and humidity data in the observational vector. This indeed caused the disappearance of the vertical lines in Fig.R8b, c (not shown).

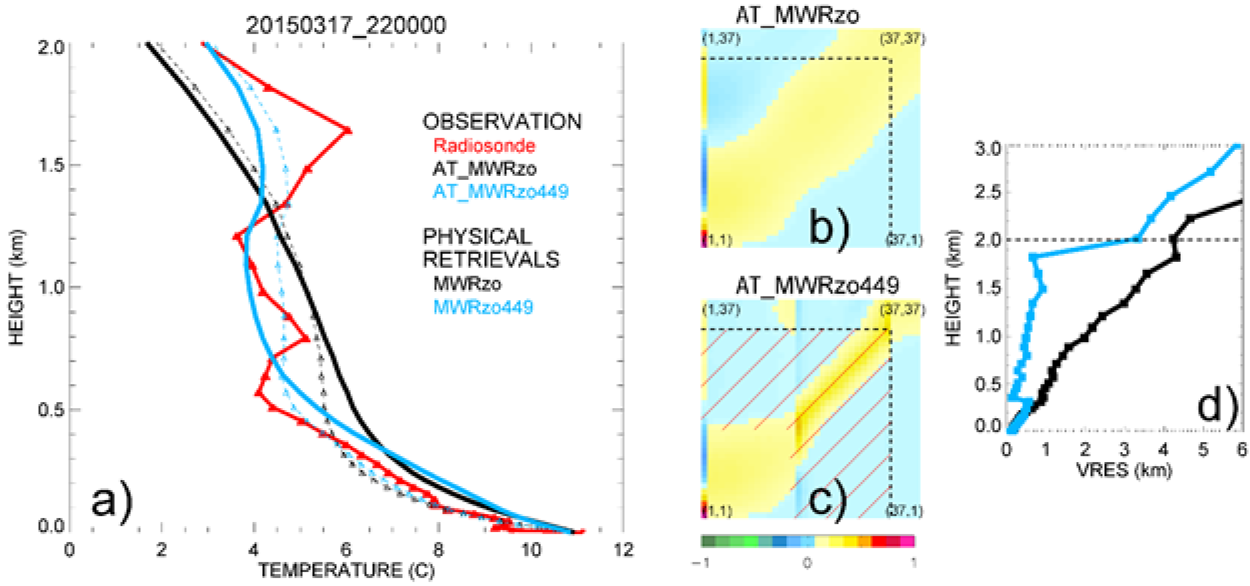

Fig. R8. The same as Fig.3 in the manuscript with two changes: T radiosonde profiles smoothed by AT_Kernel in MWRzo (dashed black) and MWRzo449 (dashed light-blue) are included in panel a), panel d) shows Vertical resolution calculated by FWHM method. These changes are included in the manuscript.

We also change the panel d) in this Figure by changing the method used to calculate the vertical resolution. There are two ways to compute the vertical resolution from the averaging kernel.

First, we applied a method that Tim Hewison published (TGRS 2007, reference below) that uses only the diagonal data of the averaged kernel. This method works well when the retrieval uses only the input from the passive observations, like the MWR, but is not very suitable for the passive/active combination of inputs, as was seen in Fig. 3d in the manuscript (with the creation of the “jumps”). So, we returned to the method (that we actually erroneously mentioned in the paper) that computes the vertical resolution as the full-width half-maximum (FWHM, TGRS 2008, reference below) value of the averaging kernel at each height.

T. J. Hewison, "1D-VAR Retrieval of Temperature and Humidity Profiles From a Ground-Based Microwave Radiometer," in IEEE Transactions on Geoscience and Remote Sensing, vol. 45, no. 7, pp. 2163-2168, July 2007, doi: 10.1109/TGRS.2007.898091.

Maddy, E. S. and C. D. Barnet, 2008: Vertical Resolution Estimates in Version 5 of AIRS Operational Retrievals. IEEE TGRS, VOL. **46**, NO. 8, AUGUST 2008, doi:10.1109/TGRS.2008.917498

Section 3.3, line 437 : change dash lines into dashed lines.
Changed.

Section 4.1, line 468 : to be consistent add a space to 1km => 1 km
Added.

Section 3.3, figure4 : can you explain why MWRzo915 does not make any improvement of the vertical resolution above ~600m compared to the MWRzo ? From panel c) it seems the spread around the diagonal is significantly reduced compared to MWRzo. However, the black and purple lines are almost on top of each other in panel e).

The reason why the vertical resolution of the MWRzo915 is very similar to that of the MWRzo above ~750m is explained by the fact that above this height much fewer RASS measurements are available (as in fact presented in Fig. 10), therefore the positive impact brought by the inclusion of RASS measurements is greatly reduced above that height.

Section 4.1, line 479 : change dash lines into dashed lines.

Changed.

Section 4.1, line 531 : add a space to « 5 km » to be consistent through the manuscript.

Added.

Section 4.1, line 535 : change as good as that during XPIA into « as good as during XPIA ».

Deleted “that”.

Section 4.2, line 544 : please changed into « smoothed radiosonde using the averaging kernel matrix ».

Changed.

Section 4.2, line 566 : change « above and below 1.5 km » into « by up to 5 km AGL »

We think it is important to refer to the 1.5 km height because this is the maximum height reached by most of the RASS measurements.

Section 4.2, line 567 : change statistical measures into statistical scores.

Changed.

Section 4.2, line 567 : I do not understand this sentence which is in contradiction with the previous one. Line 566 you mention that statistical scores are very different for all PRs but then line 567 that above 1.5 km AGL they are similar. What do you mean? Please correct the text accordingly.

There is no contradiction in these lines. We use a separation level 1.5 km to highlight the different behavior of the scores: all profiles are more smoothed and uniform above 1.5 km (with MWRzo449 having the best RMSE and BIAS) but less so closer to the surface.

Section 4.2, line 570 : Please change « NN retrievals are very variable » into « the accuracy of NN retrievals is very variable ».

Changed.

Section 4.2, line 571 : Your conclusion is only true above 1 km altitude, below 1 km altitude, NN retrievals perform better than MWRz and MWRzo and even the two configurations with RASS measurements. The degradation of NN retrievals above 1 km is mainly due to a large bias which might be due to the fact that you do not apply the bias correction to MWR measurements for NNs whereas you apply it to the PRs. This needs to be justified and clearly stated here. Linked to my previous comment, I do not understand how NN retrievals can be improved below 1 km with oblique measurements whereas you concluded in section 4.1 that oblique measurements present a large bias. Additionally, the MWRz using only zenith measurements also present a large bias (above 1 K) below 1 km altitude which seems to conclude that probably opaque channels are biased both at zenith and oblique measurements. Could you also comment on the degradation of the accuracy of MWRzo915 between ~ 200 m and 1 km ? In figure 5 you showed an example were the RASS 915 measurements were able to improve temperature retrievals of MWRz and MWRzo above 200m but averaged over all the profiles it is not the case any more. It seems to come from a bias in your retrieval that we do not observe with MWRzo 449.

Comparison to NN profiles are moved to Appendix A where the reviewer's questions have been addressed.

The degradation of MWRzo915 above 200m is also seen in Fig. 10 of the manuscript. While the availability of RASS 449 data is almost constant from 300m to 1.6 km, RASS 915 data availability faded quickly in height with its reduction from 100% availability at 300 m to almost 10% at 1km.

Fig. 5 shows the most complicated temperature profile during XPIA, it is also a very interesting case in terms of all possible active measurements' availability, from both RASS 499 and RASS 915.

Section 4.2, figure 6 : I think the vertical blue and red lines to identify a correlation of « 1 », perfect
RMSE of 0 and bias of zero are confusing for me. The figure being already crowded, I would
remove these additional coloured lines for only a vertical black dashed line for panels c and f only.

Vertical lines in Fig. 6 will be changed to black in the new version.

Section 4.2, figure 7 : I am surprised that you use oblique measurements from the MWR for
humidity retrievals: can you comment on the fact that this probably violates the homogeneity
assumption necessary to use low elevation angles? In general, only opaque channels are used at low
elevation angles and they are not sensitive to water vapor. If you used low elevation angles, did you
apply a quality-control to detect inhomogenous cloudy scenes ?

Tb obliques data are used as an average from two scans, 15 and 165. We note that most of the radiosonde launches were made in periods without liquid clouds, so the oblique scans should be similar. Also, the K-band channels from the oblique scans are not used in the retrieval, thus spatial variability in water vapor is not an issue. We only use the more opaque V-band channels for the oblique scans. Therefore we believe that our calculation of humidity retrievals is valid.

Section 4.3, line 620 : what do you mean by « weighted average over the 42 vertical heights » ?

The following text is included in the text:

"The vertical resolution of the Physical Retrievals is not uniform, with more frequent levels closer to the surface. If the data from all levels are used as the simple average, the near-surface layer will be weighted more compared to the upper levels of the retrievals. To avoid this, a vertical averaging in 0-5 km profiles is performed with separate weights at each vertical level calculated by the distance between the levels."

This is a very common validation procedure over some slice of the model with uneven vertical resolution.

Section 4.3, figure 8 : Could you comment about the potential modifications to your figure if you
had calculated the statistics up to 1 km or 2 km AGL instead of 5 km ?
As you do not apply a bias correction to the NN retrievals where V-band transparent channels have
a strong bias I am wondering if the conclusions are not wrongly biased for the evaluation of NN

retrievals with this averaging up to 5 km. As already mentionned previously, it is not fair to
compare two retrievals not applied on the same dataset (one with bias correction, another one
without). At least this should be again commented when discussing the results of this section.

We made the statistical evaluation of temperature profiles up to 1, 2 and 5 km heights (see Fig. R9).

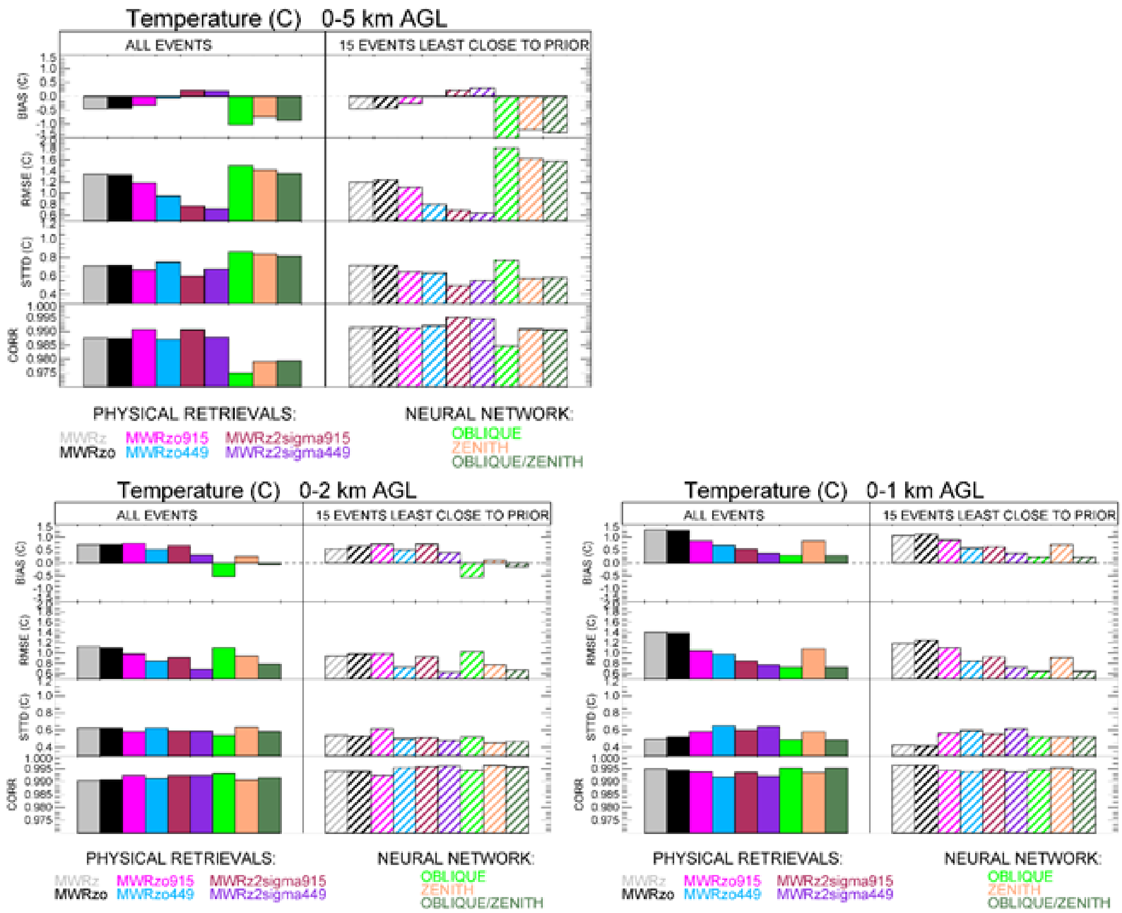

Fig. R9. On each double-panel plot from top to bottom: biases (retrievals minus ATkernel radiosonde), RMSEs, standard deviations of the difference between retrievals and ATkernel radiosonde, and Pearson correlations for the six PR configurations and three NN retrievals, oblique, zenith and their combination, averaged from the surface to 5 km AGL (top), to 2 km AGL (bottom left) and to 1 km AGL (bottom right), and averaged over the 15 events furthest from the priors (hatched boxes).

Statistical analysis shows similar behavior for the PR configurations in terms of RMSE for all three vertical layers. For NN statistics, we included a third type of comparison against the radiosonde measurements, the combination of the oblique scan temperature profiles up to 1 km AGL and the zenith scan temperature profiles above 1km AGL. This combined NN has the lowest RMSE compared to the other two NN scans considered separately. Also, these combined NN profiles have the lowest RMSE in the lower layer of 0-1 km compared to all PR profiles, but larger RMSE in wider atmospheric layers such as 0-2 or 0-5 km. All three NN retrievals (oblique only, zenith only, oblique and zenith combined) have the highest RMSE compared to all PR configurations in the layer of the atmosphere up to 5 km. From the PR temperature profiles, the RMSE decreases from the passive instrument configurations (MWRz, MWRzo) to the configurations with active RASS measurements in very similar ways over the 0-5, 0-2, and 0-1 km atmospheric layers, especially when comparing the 0-1 and 0-5 km layers of the atmosphere. Bias also improves from MWRz/MWRzo to the configurations that include RASS. The setting of MWRz2sigma449 shows the best statistics in terms of bias and RMSE compared to all other PR retrievals, and better to all three NN retrievals in 0-2 and 0-5 km layers. In general, almost all PR profiles with RASS have RMSE below 1 K in all three vertical layers.

Conclusion line 703 : I honestly did not have understand that NN retrievals with oblique measurements do not use the zenith observation. This has to be more explicit directly in section 2.1, line189 to 201. This explanation arrives too late in the manuscript

Comparison to NN profiles are moved to Appendix A, where we clarified the difference between the NN configurations.

Conclusion : line 718 when MonoRTM is mentioned is redundant with line 719. I suggest modifying lines 717 to 719 into :

the small systematic errors that exist between the MWR observed Tb values and the RASS measurements and (b) the systematic errors that exist in forward microwave radiative models.

(I would thus remove all the text between parentheses).

Modified.

Conclusion, line 722 : please correct the most difficult to retrieve and the most important to forecast.

Corrected.

Conclusion, line 728: this sentence should be mitigated : the study proves that active sensors can improve MWR passive observations with zenith observations only but due to the weird results you obtain with lower elevation angles which are expected to improve the retrievals in the same area as the RASS measurements I think you should mention that the results could be different with MWRs

with elevation angles usable down to 5° above the ground. In fact, with new MWR instruments
using both zenith and low elevation angles we can expect RMSE between 0.5 and 1.5 K in the first
2 km (1.5 K for cloudy-scene when there is a temperature inversion in the upper layers). Thus, we
cannot be sure that the improvement brought by RASS measurements would be as much
informative in the first 1 km with a MWR unit for which oblique measurements could be optimally
used. I think you should mention this in your conclusion.

The text in the manuscript is modified as:

"Even for this subset of selected cases we find that MWRz2sigma449 produces better statistics, proving that the inclusion of active sensor observations in MWR passive observations would be beneficial for improving the accuracy of the retrieved temperature profiles also in the upper layer of the atmosphere where RASS measurements are not available (at least up to 5 km AGL). However, we note that this result may be dependent on the fact that our oblique measurements were taken at a 15 degree elevation angle, and that MWRs in locations with unobstructed views allowing for scans down to 5 degrees may provide similar improved accuracy to the temperature profiles (reference below) in 0-1 or even 0-2 km AGL layers."

Crewell, S., U. Löhnert, 2007: Accuracy of Boundary Layer Temperature Profiles Retrieved With Multifrequency Multiangle Microwave Radiometry, IEEE TGRS, VOL. 45, NO. 7, JULY 2007, **DOI:** 10.1109/TGRS.2006.888434

Reviewer #2, answers.

We thank the reviewer for reading our manuscript and for offering many useful comments towards its improvement. In the revised manuscript, we included modifications addressing almost all of these comments.

The submitted manuscript takes up on the ground-based remote sensing synergy approach of combining microwave radiometers (MWR) and RASS by applying a state-of-the-art physical retrieval approach. This is important, since MWR are known to show very accurate performance in temperature profiling in the lowest 500 m, whereas RASS are able to adequately capture the typical temperature inversion at the top of the atmospheric boundary layer (ABL) and thus, in theory, the synergy of both could lead to an improved temperature profile throughout the whole ABL.

Major points

1.) The way to showing the latter point above, however, is obviously severely hampered by the quality of the MWR data, most probably in terms of a TB bias. While the authors do show a bias correction applied to the MWR TBs, it is unclear whether this was done only for zenith observations or also at 15° elevation (Fig. 1). Here a detailed analysis is missing. If this manuscript is to be accepted for publication using real TBdata, the reason for the biases shown in Figs. 6 c and f (black a grey lines) must be identified, discussed and corrected for.

We thank the reviewer for this specific comment. Some parts of the bias-correction description were indeed missing. Additional text has been included in Section 3.2: "We compute the bias in the bias-correction procedure only from the zenith scans assuming that the same bias is suitable for the oblique scans. Also, we use the assumption that the true bias is an offset that is independent of the scene, so that the sensitivity to the scene (e.g., clear or cloudy, zenith or off-zenith) is small. To investigate this, we eliminated the radiosondes launched during rainy periods (5 out of 58 cases) and found that the averaged temperature profiles were very little different than when all radiosonde profiles."

More detailed discussion of the temperature biases shown in Fig. 6, especially near the surface layer, will be included in Section 4.2 in the final version of the manuscript.

2.) The paper shows hardly any quantitative discussion, which is necessary for a sound scientific analysis. Except for just a few passages, discussions of the figures are carried out only in a qualitative, rather unspecific manner. With respect to this, specifically the sections 3 and 4 should be thoroughly rewritten. E.g., avoid using "This might..", "We believe…", "seemingly", "Differences", "better" or "improve" etc.

without referring to adequate statistical measures. A lot of the data is there in the XPIA data set und you can use to confirm, deny or to quantify your assumptions, respectively results.

We have tried to avoid purely qualitative descriptions, and to provide quantitative details in the indicated sections for the new version of the manuscript, thank you.

For ex., in Section 3, especially 3.2, we included the detailed descriptions of how the clear-sky days were chosen and how the uncertainty and the bias for each MWR channel were calculated.

3.) Because the authors write they could not apply any bias correction to the NN approaches, I strongly suggest omitting them from the paper. The comparisons are thus “unfair” and I do not see what benefit the reader has from including the NN retrievals when the actual goal is evaluating the MWR/RSS synergy potential that can be achieved with the PR. Instead, in all the corresponding figures, I would like to see

the results of RSS-only PR, i.e. without including the MWR so the reader has an impression what these systems are capable of in a stand-alone manner.

We thank the referee for this particular comment. Following your recommendation and also the opinion of Reviewer #1 on this matter, we decided to move all comparisons of PR and NN profiles to Appendix A, while also making note of the fact that without mentioning NN retrievals our analysis would be incomplete for the community of MWR end-users. We think that the possibility to do the bias correction in the PR is just one of the advantages the PR has. The NN retrievals are provided by the manufacturer and have the disadvantage that no bias correction is performed. They are nevertheless used by most end-users. We believe that the comparison between PR and NN is still very important and should be included in some way in the manuscript, while noting the unequal basis for the NN and bias-corrected PR comparison. These issues are now addressed in the Appendix.

Regarding a RASS-only PR, we do not see the value of this because RASS without MWR in MonoRTM will be used as RASS + prior, so we should get mostly the profile of the prior because the RASS covers only a small portion of the 17 km temperature profile. On the other hand, the RASS measurements are included in the figures, especially in Fig. 10 in the manuscript, showing what these instruments can provide in a stand-alone manner.

4.) How did you deal with clouds, what about precipitation? Did you retrieve LWP simultaneously to temperature and water vapor? What influence do clouds have on the retrieval? I find no information about this throughout the manuscript.

Most of the radiosondes were launched during clear-sky time. See also answers to Referee #1 about this.

We included several new paragraphs in Section 3.2, e.g.:

“we found that from 58 radiosonde launches used in our statistical analysis, 41 belong to the clear-sky category, 12 - to cloudy but non-precipitating conditions and 5 - to rainy periods”.

A discussion of the impacts of clouds on the retrieval is mentioned in comment 1) above and will be included in the manuscript.

5.) The sections describing microwave radiometry need more background and scientific accuracy.

We had already included many references in order to avoid a detailed description of the basic principles of microwave radiometry.

Further specific points and questions to be addressed

1.) Abstract, last paragraph: It is not clear if the improvements described refer to the PR compared to the NN or the MWR+RASS combination compared to the MWR-only retrieval.

As we moved the discussion of PR and NN profiles comparison in Appendix A, this paragraph has been changed to highlight the purpose of this paper as:

"Having the possibility to combine the information provided by the MWR and RASS systems, in this study the physical-iterative approach is tested with different observational inputs: first using data from surface sensors and the MWR in different configurations, and then including data from the RASS. These temperature retrievals are assessed against 58 co-located radiosonde profiles. Results show that the combination of the MWR and RASS observations in the physical-iterative approach allows for a more accurate characterization of low-level temperature inversions compared to the physical retrievals of the MWR passive measurements, and that these retrieved temperature profiles match the radiosonde observations better than the temperature profiles retrieved from the MWR in the atmospheric layer between the surface and 5 km AGL. Specifically, in this layer of the atmosphere, both root mean square errors and standard deviations of the difference between radiosonde and retrievals that combine MWR and RASS are improved by ~0.5 K compared to the difference between radiosonde and MWR retrievals. Pearson correlation coefficients are also improved.

We provide the comparison of the temperature physical retrievals to the neural network retrievals in Appendix A."

2.) Introduction: A description of the physical principle that allows temperature (& humidity) profiling (and LWP retrieval) from passive MWR observations is missing. When doing so, please consider reformulating the advantages and disadvantages of the MWR retrieval methodology, because they are currently not scientifically sound.

Be sure to differentiate how the frequency dependence and elevation angle dependence of TB can both lead to resolving the temperature profile in the vertical.

We are not sure what the Reviewer is suggesting here. There are many articles describing the MWR temperature and humidity retrievals as well as physical principles of such retrievals, and we had already included many of these references in the manuscript in order to avoid a detailed description of the basic principles of microwave radiometry.

Nevertheless, we include a description of the temperature retrieval frequencies in Section 2.1:

"V-band frequencies or channels also could be divided in two categories: the opaque channels, 56.66 GHz and higher, which are more informative in the low layer of the atmosphere from the surface to ~1 km above the ground and the transparent channels, 51-56 GHz, which are more informative above 1 km in the temperature profile".

3.) Line 109: MWR don't "apply radiative transfer equations and neural network retrievals…" – please reformulate.

This paragraph is reformulated to: "Radiative transfer equations are commonly used to train statistical retrievals or as forward models within physical retrieval methods".

4.) Line 115: Please make clear what you mean with "deep layer of the atmosphere".

Changed to: "the layer of the whole troposphere ".

5.) Section 2.1, lines 203-204: The purpose of using observations at 15° elevation is not to "average out small scale horizontal inhomogeneities of the atmosphere" but to obtain TB observations at different optical depths.

This paragraph has been modified according to your suggestion:

"In this study we make use of the NN zenith and of the NN oblique measurements, where the latter can obtain TB observations at different optical depths."

6.) Section 3.1, lines 280-286: Why does the Y vector and the error covariance matrix contain both "zenith" and "zenith+oblique" components. If I understand correctly, you can choose to use only zenith observations and add the off-zenith (=oblique) TBsto improve the retrieval? So then should it not be "zenith" and "oblique"? Please clarify.

Table 1 as well as observational vectors Y2, Y3 and Y4 and matrix Sε are modified:

	T_{sfc}	Q_{sfc}	Tb_{zenith}	$Tb_{oblique\_avrg}$	$Tv_{RASS915}$	$Tv_{RASS449}$
$\boldsymbol{Y_1}$ = *MWRz*	*X*	*X*	*X*			
$\boldsymbol{Y_2}$ = *MWRzo*	*X*	*X*	*X*	*X*		
$\boldsymbol{Y_3}$ = *MWRzo915*	*X*	*X*	*X*	*X*	*X*	
$\boldsymbol{Y_4}$ = *MWRzo449*	*X*	*X*	*X*	*X*		*X*

$$\mathbf{Y}_1 = \begin{bmatrix} T_{sfc} \\ Q_{sfc} \\ \boldsymbol{Tb}_{zenith} \end{bmatrix} \qquad \mathbf{Y}_2 = \begin{bmatrix} T_{sfc} \\ Q_{sfc} \\ \boldsymbol{Tb}_{zenith+oblique\ avrg} \end{bmatrix}$$

$$Y_3 = \begin{bmatrix} T_{sfc} \\ Q_{sfc} \\ \boldsymbol{Tb_{zenith+oblique\ avrg}} \\ \boldsymbol{Tv_{RASS915}} \end{bmatrix} \qquad Y_4 = \begin{bmatrix} T_{sfc} \\ Q_{sfc} \\ \boldsymbol{Tb_{zenith+oblique\ avrg}} \\ \boldsymbol{Tv_{RASS449}} \end{bmatrix}$$

$$\boldsymbol{S_\varepsilon} = \begin{bmatrix} \sigma^2_{Tsfc} & 0 & 0 & 0 \\ 0 & \sigma^2_{Qsfc} & 0 & 0 \\ 0 & 0 & \boldsymbol{\sigma^2_{Tb_{zenith}}}\ (1)\ \boldsymbol{or}\ \boldsymbol{\sigma^2_{Tb_{zenith+oblique\ avrg}}}\ (2) & 0 \\ 0 & 0 & 0 & \boldsymbol{\sigma^2_{Tv_{RASS915(449)}}}\ (3\text{ or }4) \end{bmatrix}$$

7.) Line 310: Do you mean the covariance between the uncertainties of the measurements?

This part of the manuscript is reformulated:

"The uncertainty in the MWR Tb observations was set to the standard deviation from a detrended time-series analysis for each channel during cloud-free periods. The derived uncertainties ranged from 0.3 to 0.5 K in the 22 to 30 GHz channels, and 0.5 to 1.0 K in the 52 to 60 GHz channels. We assumed that there was no correlated error between the different MWR channels.

For the RASS, collocated RASS and radiosonde profiles were compared and the standard deviation of the differences in Tv were determined as a function of the radar's signal-to-noise ratio (SNR). This relationship resulted in uncertainties that ranged from 0.8 K at high SNR values to 1.5K at low SNR values. Again, we assumed that there was no correlated error between different RASS heights. Following all these assumptions, the covariance matrix $\mathbf{S_\varepsilon}$ is diagonal."

8.) Section 3.2: There seems to be a non-consistent use of terminology. Please use "uncertainty" only in the sense of random uncertainty and distinguish it clearly from systematic offset (=bias).

We have made certain to consistently refer to the random uncertainty of Tb as the uncertainty, and the systematic offset as the bias.

9.) Lines 323-324: erroneous, please reformulate in a consistent manner

The text is changed as:

"While the bias of the retrieval depends on both the sensitivity of the forward model and the observational systematic offset, we can try to eliminate, or at least to reduce, the systematic error in the MWR observations."

10.) Line 327: The 30 GHz channel is not predominantly water vapor, but liquid water sensitive.

Changed.

11.) Lines 328-330: "The random uncertainty in brightness temperature was calculated as its standard deviation during clear sky times and for this channel is approximately 0.3 K": Why is this calculated standard deviation related to the TB uncertainty? Over what time window did you average? What about water variability in the atmosphere during the calculation time? Why actually did you calculate this standard deviation and where do you use it in the course of your study?

Thank you for this comment. We included a much more detailed description of the uncertainty calculation in the text in Section 3.2:

"A threshold value of 0.3 K has been used for the uncertainty calculation. The random uncertainty in Tb is calculated as an average of the Tb standard deviation in a one hour sliding window through all data points of a day. It also could be computed as the standard deviation of the difference between Tb and the smoothed Tb to eliminate daily temperature variability. Finally, there is a "standard" set of uncertainties used as the high boundaries for Tb uncertainty per MWR channels calculated empirically in the previous experiments. Four clear-sky days have been chosen using a criterion of 0.3 K uncertainty in the 30 GHz channel: March 10 and 30, and April 13 and 29, 2015.

During periods with liquid-bearing clouds overhead, this criterion is markedly higher (more than 0.7 K) and much higher for the rainy periods (> 4 K). While those calculations were applied on a daily basis, it is important to mention that the days are not uniform in terms of cloudiness or rain. Therefore, we used the data for the 2-3 hours bracketing the time of radiosonde launches to determine to which category a particular radiosonde profile belongs, clear-sky, cloudy or rain. In this way, we found that from 58 radiosonde launches used in our statistical analysis, 41 belong to the clear-sky category, 12 - to cloudy but non-precipitating conditions and 5 - to rainy periods. For the four chosen clear-sky days not only were the daily uncertainties of 30 GHz Tb below 0.3 K, but all three sets of uncertainties described above were extremely similar with the averaged difference less than 0.05 K."

12.) Lines 332-333: How were the clear-sky days selected?

Please, see above.

13.) Lines 333-334: How did you calculate the bias?

From the modified text in Section 3.2:

"The bias was computed for each of the 22 channels as the averaged difference between the observed Tb from the MWR zenith observations, and the forward model calculation applied to the prior, over these selected clear-sky days, and then subsequently removed from all of the MWR observations."

14.) Before line 358: a description and a quantitative discussion of the Sa and Se matrices applied needs to be given before going on describing retrieval results.

Sa and Se matrices are described in Section 3.1 and retrieval results are discussed in 3.2.

15.) Lines 425 and following, referring to Fig. 3: quantitative argumentation missing and VRES "jumps" in Fig. 3 are not discussed

We thank the Reviewer for this comment very much because it prompted us to reconsider the method used to calculate the vertical resolution.

There are two ways to compute the vertical resolution from the averaging kernel. First, we applied a method that Tim Hewison published (TGRS 2007, reference below) that uses only the diagonal data of the averaged kernel. It works well when the retrieval uses only the input from the passive observations, like the MWR, but is not very suitable for the passive/active combination of inputs, as is seen in Fig. 3d in the manuscript (with the creation of the "jumps"). So, we returned to the method (that we actually erroneously mentioned in the paper) that computes the vertical resolution as the full-width half-maximum (FWHM, Maddy and Barnet, TGRS, 2008, reference below) value of the averaging kernel at each height.

T. J. Hewison, "1D-VAR Retrieval of Temperature and Humidity Profiles From a Ground-Based Microwave Radiometer," in IEEE Transactions on Geoscience and Remote Sensing, vol. 45, no. 7, pp. 2163-2168, July 2007, doi: 10.1109/TGRS.2007.898091.

Maddy, E. S. and C. D. Barnet, 2008: Vertical Resolution Estimates in Version 5 of AIRS Operational Retrievals. IEEE TGRS, VOL. **46**, NO. 8, AUGUST 2008, doi:10.1109/TGRS.2008.917498

Using the FWHM method, Fig.3 is changed to the one below, where the "jumps" in panel d are significantly reduced:

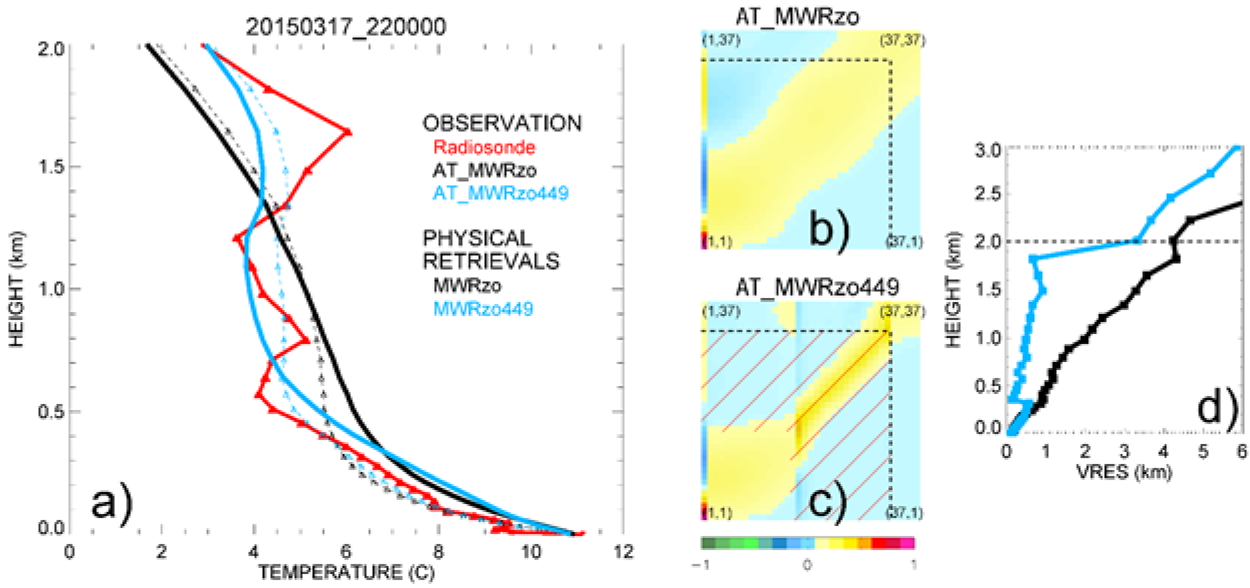

16.) Section 4.1, lines 469-471: unspecific sentence, please reformulate

This sentence is deleted because soon after the similar text is followed:

"MWRzo449 has the best statistical measures compared to the other PRs, particularly below 2 km AGL, where RASS 449 measurements are available".

17.) Fig. 5: How many cases are used for the statistics, how many are clear-sky, how many are cloudy sky? How did you deal with cloudy cases in general?

Statistical results are shown in Figs. 4, and 6-10, not in Fig. 5 of the manuscript (where a single case profile - 18 March, 2015 at 0200UTC is presented). For the statistical analysis, from 58 valid radiosonde profiles 41 have been launched in clear-sky periods, 12 - in cloudy but non-precipitating conditions and 5 - in rainy time. This information is now included in the manuscript, Section 3.2. We defined those categories using the 30 GHz channel Tv as in these figures:

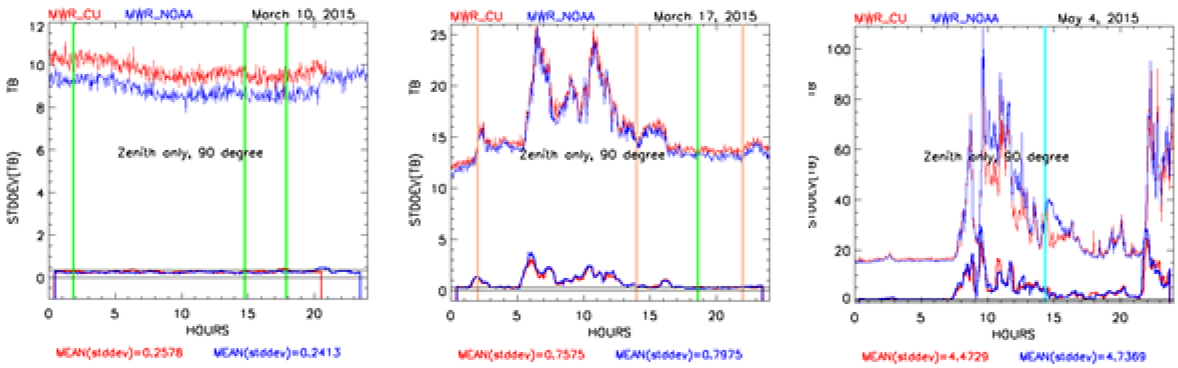

Zenith Tb from a 30 GHz channel for a clear-sky day (left panel), cloudy day (middle panel) and rainy day (right panel) from the CU radiometer in red and NOAA radiometer in blue. STDDEV(Tb-SMOOTH(tb,11)) is shown at the bottom in each panel with its average values printed under the panels in corresponding colors. Vertical (green – for clear-sky, beige – for clouds and cyan – for rain) lines show the time of radiosonde launches.

18.) Fig. 8: Can you derive meaningful statistical measures such as RMSE from only 15 cases?

This is a valid comment. We are interested in describing the “worst case” most extreme events, when the radiosonde temperature profiles are most different from the prior profile, and so, by definition the number of cases needs to be limited, otherwise they are no longer extreme. On the other hand, some level of statistical significance is desired. Given that we have 58 radiosondes, 15 events are already nearly 25% of the total. We felt that this was a reasonable compromise given the limitations of the data set.

19.) Fig. 9: The MWRz2sigma449 performs best compared to the other retrievals. This retrieval relies on an increase in the MWR uncertainty, which was chosen in an arbitrary manner. This choice should be thoroughly justified and set into context with the performance of the 449-only retrievals which I would like to see (see “Major points” above).

The choice of double MWR uncertainty for MWRz2sigma449 is not arbitrary, but the reviewer is absolutely right, it is not qualitatively justified in the manuscript. It was chosen based on the “worst” XPIA temperature profile on March 18, 2015, 02:00 UTC showing in Fig.5

in the manuscript. This particular case is not only the worst in the XPIA experiment in terms of temperature inversions (three of them in one profile, with one near the surface), but with other complications. We found that the MWR Tb from the opaque channels of both zenith and obliques scans, have biases (to the forward model calculation of radiosonde Tb) of around 1 K. We wanted to check our hypothesis about too little freedom of the PR approach in the layer between surface and RASS measurements. As is mentioned in the text, “After several trials”, we indeed made many additional runs, but we wanted to keep our recommendations general, and not be very specific about this particular case.

20.) Section 4.4, lines 683-686: This sentence is formulated in a general, rather nonspecific way and could be given without any of the studies conducted here.

This paragraph is removed.

Technical comments

1.) Figures are given in rather low resolution, a higher one would have been nice to be able to better interpret the results.

All figures are in tiff format that has a high resolution. The deterioration of the images comes from the conversion to PDF. Original tiff format files will be provided to the editorial office when requested.

2.) Equation fonts appear in a non-standard, unorganized way.

Equation font is changed to be the same throughout the paper.

3.) In general: please write K or °C, but not °K.

Checked and fixed.

4.) Section 3.1, lines 280-286: Numerate all equations, be consistent with equation fonts and text fonts, be consistent with variables (i.e. L, LWP), explain all variables (and indices) in the text. Please be neater.

Lines 280-286 consist of only one equation, Eq. (1), which is numbered, and the descriptions of all its terms. We changed the text to have consistency in fonts and text fonts, and we consistently used LWP in the revised text.

5.) Line 348 and following: use a new sub-section, the paragraphs are not related to “Bias-correction” anymore

We renamed the Section **3.2 PR’s bias-correction** to **3.2 PR’s bias-correction and PR’s temperature profiles.**

6.) Section 3.3, lines 415-421: move text to Fig. 3 caption

The text on these lines reformulates the Fig. 3 description in a more explanatory way.

Improving thermodynamic profile retrievals from microwave radiometers by including Radio Acoustic Sounding System (RASS) observations

Irina V. Djalalova[1,2], David D. Turner[3], Laura Bianco[1,2],

James M. Wilczak[2], James Duncan[1,2]~~,~~[*], Bianca Adler[1,2] and Daniel Gottas[2]

[1] Cooperative Institute for Research in Environmental Sciences (CIRES), Boulder, CO, USA

[2] National Oceanic and Atmospheric Administration, Physical Sciences Laboratory, Boulder, CO, USA

~~[3]National~~[3] National Oceanic and Atmospheric Administration, Global Systems Laboratory, Boulder, CO USA

Formatted: *Font color: Auto*

~~Draft: in preparation for Journal of Atmospheric Measurement Techniques (12/18/2020)~~

[*]Now at WindESCo, Burlington, MA

Formatted: *Space After: 12 pt, Line spacing: Double, Border: Top: (No border), Bottom: (No border), Left: (No border), Right: (No border), Between : (No border)*

Corresponding author address: Irina V. Djalalova (Irina.V.Djalalova@noaa.gov), NOAA/Physical Science Laboratory, 325 Broadway, mail stop: ~~-~~PSD3, Boulder, CO 80305. Tel.: 303-497-6238. Fax: 303-497-6181.

Outline

Formatted: *Outline numbered + Level: 1 + Numbering Style: 1, 2, 3, … + Start at: 1 + Alignment: Left + Aligned at: 0" + Indent at: 0.25"*

Formatted: *Outline numbered + Level: 1 + Numbering Style: 1, 2, 3, … + Start at: 1 + Alignment: Left + Aligned at: 0" + Indent at: 0.25"*

Formatted: *Outline numbered + Level: 2 + Numbering Style: 1, 2, 3, … + Start at: 1 + Alignment: Left + Aligned at: 0.25" + Indent at: 0.5"*

Formatted: *Outline numbered + Level: 1 + Numbering Style: 1, 2, 3, … + Start at: 1 + Alignment: Left + Aligned at: 0" + Indent at: 0.25"*

Formatted: *Space After: 12 pt, Line spacing: Double, Border: Top: (No border), Bottom: (No border), Left: (No border), Right: (No border), Between : (No border)*

Abstract

Thermodynamic profiles are often retrieved from the multi-wavelength brightness temperature observations made by microwave radiometers (MWRs) using regression methods (linear, quadratic approaches), artificial intelligence (neural networks), or physical-iterative methods. Regression and neural network methods are tuned to mean conditions derived from a climatological dataset of thermodynamic profiles collected nearby. In contrast, physical-iterative retrievals use a radiative transfer model starting from a climatologically reasonable value of temperature and water vapor, with the model run iteratively until the derived brightness temperatures match those observed by the MWR within a specified uncertainty.

In this study, a physical-iterative approach is used to retrieve temperature and humidity profiles from data collected during XPIA (eXperimental Planetary boundary layer Instrument Assessment), a field campaign held from March to May 2015 at NOAA's Boulder Atmospheric Observatory (BAO) facility. During the campaign, several passive and active remote sensing

Formatted: *Outline numbered + Level: 1 + Numbering Style: 1, 2, 3, … + Start at: 1 + Alignment: Left + Aligned at: 0" + Indent at: 0.25"*

Formatted: *Space After: 12 pt, Line spacing: Double, Border: Top: (No border), Bottom: (No border), Left: (No border), Right: (No border), Between : (No border)*

instruments as well as in-situ platforms were deployed and evaluated to determine their suitability for the verification and validation of meteorological processes. Among the deployed remote sensing instruments was a multi-channel MWR, as well as two radio acoustic sounding systems (RASS), associated with 915-MHz and 449-MHz wind profiling radars.

Having the possibility to combine the information provided by the MWR and RASS systems, in this study the physical-iterative approach is tested with different observational inputs: first using data from surface sensors and the MWR in different configurations, and then including data from the RASS. These temperature retrievals are ~~also compared to those derived by a neural network method, assessing their relative accuracy~~assessed against 58 co-located radiosonde profiles. Results show that the combination of the MWR and RASS observations in the physical-iterative approach allows for a more accurate characterization of low-level temperature inversions, and that these retrieved temperature profiles match the radiosonde observations better than ~~all other approaches, including~~ the ~~neural network~~temperature profiles retrieved from only the MWR, in the ~~atmospheric~~ layer between the surface and 5 km above ground level (AGL~~.~~). Specifically, in this layer of the atmosphere, both root mean square errors and standard deviations of the difference between radiosonde and retrievals that combine MWR and RASS are improved by ~0.5 °C compared to the other methods. Pearson correlation coefficients are also improved.

Formatted: *Font: Calibri, 12 pt, Font color: Auto, Not Highlight*

Formatted: *Space After: 12 pt, Line spacing: Double, Border: Top: (No border), Bottom: (No border), Left: (No border), Right: (No border), Between : (No border)*

We provide the comparison of the temperature physical retrievals to the neural network retrievals in Appendix A.

1. Introduction

To monitor the state of the atmosphere for process understanding and for model verification and validation, scientists rely on observations from a variety of instruments, each one having its set of advantages and disadvantages. Using several diverse instruments allows one to monitor different aspects of the atmosphere, while combining them in an optimized synergetic approach can improve the accuracy of the information we have on the state of the atmosphere.

During the eXperimental Planetary boundary layer Instrumentation Assessment (XPIA) campaign, an U.S. Department of Energy sponsored experiment held at the Boulder

Formatted: Outline numbered + Level: 1 + Numbering Style: 1, 2, 3, … + Start at: 1 + Alignment: Left + Aligned at: 0.25" + Indent at: 0.5"

Formatted: Space After: 12 pt, Line spacing: Double, Border: Top: (No border), Bottom: (No border), Left: (No border), Right: (No border), Between : (No border)

Atmospheric Observatory (BAO) in Spring 2015, several instruments were deployed (Lundquist et al., 2017) with the goal of assessing their capability for measuring flow within the atmospheric boundary layer. XPIA investigated novel measurement approaches, and quantified uncertainties associated with these measurement methods. While the main interest of the XPIA campaign was on wind and turbulence, measurements of other important atmospheric variables were also collected, including temperature and humidity. Among the deployed instruments were two identical microwave radiometers (MWRs) and two radio acoustic sounding systems (RASS), as well as radiosondes launches that were used for verification.

MWRs are passive sensors, sensitive to atmospheric temperature and humidity content that allow for a high temporal observation of the state of the atmosphere, with some advantages and limitations. In order to estimate profiles of temperature and humidity~~, they observe atmospheric~~ from the observed brightness ~~temperature and apply radiative transfer equations (Rosenkranz, 1998) and~~temperatures (Tb), several methods could be applied such as regressions, neural network retrievals~~ (Solheimet al., ,1998a, and 1998b; Ware et al., 2003),~~ or physical retrieval methodologies ~~that can~~which include more information about the atmospheric state in the retrieval process~~ (Turner and Blumberg, 2019).~~. Radiative transfer equations (Rosenkranz, 1998) are commonly used to train statistical retrievals, or as forward models used within physical retrieval methods. Advantages of MWRs include their compact design, the relatively high temporal resolution of the measurements (2-3 minutes), the possibility to observe the vertical structure of both temperature and moisture~~,~~ through the ~~deep layer~~depth of the ~~atmosphere that can be monitored including~~troposphere during both clear and cloudy conditions, and their capability to operate in a standalone mode.

Formatted: *Space After: 12 pt, Line spacing: Double, Border: Top: (No border), Bottom: (No border), Left: (No border), Right: (No border), Between : (No border)*

Disadvantages include ~~the~~ limited accuracy~~, as the temperature and humidity profiles are not actively measured but retrieved, their lower accuracy~~ in the presence of rain because of scattering of radiation ~~due to~~from raindrops in the atmosphere (and because ~~some~~ water can ~~still~~ deposit on the radome, although the instruments use a hydrophobic radome and force airflow over the surface of the radome during rain to mitigate this impact), rather coarse vertical resolution, and for retrievals the necessity to have a site~~-~~-specific climatology. Other disadvantages include the challenges related to performing accurate calibrations (Küchler et al., 2016, and references within), radio frequency interference (RFI), and the low accuracy on the retrieved liquid water path (LWP) especially for values of LWP less than ~~50~~20 g/m^2.

RASS, in comparison, are active instruments that emit a longitudinal acoustic wave upward, causing a local compression and rarefaction of the ambient air. These density variations are tracked by the Doppler radar associated with the RASS, and the speed of the propagating sound wave is measured. The speed of sound is related to the virtual temperature (Tv) (North et al., 1973), and therefore, RASS are routinely used to remotely measure vertical profiles of virtual temperature in the boundary layer. Being an active instrument, the RASS is in general more accurate than a passive instrument (Bianco et al., 2017), but they also come with their sets of disadvantages. The main limitations of RASS for retrieval purposes are its low temporal resolution (typically a 5-min averaged RASS profile is measured once or twice per hour), and their limited altitude coverage. Recent studies (Adachi and Hashiguchi, 2019) have shown that to make them more suitable to operate in urban areas RASS could use parametric speakers to take advantage of their high directivity and very low side lobes. Nevertheless, the maximum height reached by the RASS is still limited, being a function of both radar frequency

Formatted: *Space After: 12 pt, Line spacing: Double, Border: Top: (No border), Bottom: (No border), Left: (No border), Right: (No border), Between : (No border)*

and atmospheric conditions (May and Wilczak, 1993), and is determined both by the attenuation of the sound, which is a function of atmospheric temperature, humidity, and frequency of the sound source, and the advection of the propagating sound wave out of the radar's field-of-view. Therefore, data availability is usually limited to the lowest several ~~km, dependent~~kilometers, depending on the frequency of the radar. In addition, wintertime coverage is usually considerably lower than that in summer, due to a higher probability of stronger winds advecting the sound wave away from the radar in the winter.

To get a better picture of the state of the temperature and moisture structure of the atmosphere, it makes sense to try to combine the information obtained by both MWR and RASS. Integration of different instruments has been of scientific interest for several years (Han and Westwater 1995; Stankov et al. 1996; Bianco et al., 2005; Engelbart et al., 2009; Cimini et al., 2020~~,~~; Turner and Löhnert, 2020, to name some). In this study we particularly focus on the combination of the MWR and RASS observations in the retrievals to improve the accuracy of the temperature profiles in the lowest 5 km compared to ~~the standard MWR retrievals obtained through neural network (NN) processing, or compared to~~ physical retrieval approaches that do not include the information from RASS measurements. Some studies have used analyses from numerical weather prediction (NWP) models as an additional constraint in these variational retrievals (e.g., Hewison 2007; Cimini et al. 2005, 2011; Martinet et al. 2020); however, we have elected not to include model data in this study because we wanted to evaluate the impact of the RASS profiles on the retrievals from a purely observational perspective.

Formatted: *Space After: 12 pt, Line spacing: Double, Border: Top: (No border), Bottom: (No border), Left: (No border), Right: (No border), Between : (No border)*

This paper is organized as follows: Section 2 summarizes the experimental dataset; Section 3 introduces the principles of the physical retrieval approaches used to obtain vertical profiles of the desired variables; Section 4 produces statistical analysis of the comparison between the different retrieval approaches and radiosonde measurement; finally, conclusions are presented in Section 5.

2. XPIA data

The data used in our analysis were collected during the XPIA experiment, held in Spring 2015 (March-May) at the NOAA's Boulder Atmospheric Observatory (BAO) site, in Erie, Colorado (Lat.: 40.0451 N, Lon.: 105.0057 W, El.: 1584 m MSL). XPIA was the last experiment conducted at this facility, as after almost 40 years of operations the BAO 300-m tower was demolished at the end of 2016 (Wolfe and Lataitis, 2018). XPIA was designed to assess the capability of different remote sensing instruments for quantifying boundary layer structure, and was a preliminary study as many of these same instruments were later deployed, among other campaigns, for the second Wind Forecast Improvement Project WFIP2 (Shaw et al., 2019; Wilczak et al., 2019) which investigated flows in complex terrain for wind energy applications, and were for example used to study cold air pool and gap flow characteristics (Adler et al., ~~2020~~2021; Banta et al., 2020; Neiman et al., 2019). The list of the deployed instruments included active and passive remote-sensing devices, and in-situ instruments mounted on the BAO tower. Data collected during XPIA are publicly available at https://a2e.energy.gov/projects/xpia. A detailed description of the XPIA experiment can be

Formatted: *Outline numbered + Level: 1 + Numbering Style: 1, 2, 3, … + Start at: 1 + Alignment: Left + Aligned at: 0.25" + Indent at: 0.5"*

Formatted: *Space After: 12 pt, Line spacing: Double, Border: Top: (No border), Bottom: (No border), Left: (No border), Right: (No border), Between : (No border)*

found in Lundquist et al. (2017), while a specific look at the accuracy of the instruments used in this study can be found in Bianco et al. (2017).

2.1 MWR measurements

Two identical MWRs~~,~~ (Radiometrics MP-3000A) managed by NOAA (MWR-NOAA) and by the University of Colorado (MWR-CU), were deployed next to each other at the visitor center ~600 m south of the BAO tower (see Lundquist et al., 2017 for a detailed map of the study area). Prior to the experiment, both MWRs were calibrated using an external liquid nitrogen target and an internal ambient target and thoroughly serviced (sensor cleaning, radome replacement, etc.). MWRs are passive devices which record the natural microwave emission in the water vapor and oxygen absorption bands from the atmosphere, providing measurements of the brightness temperatures. Both MWRs have 35-channels spanning a range of frequencies, with 21 channels in the lower (22-30 GHz) K-band frequency band, of which 8 channels were used during XPIA: 22.234, 22.5, 23.034, 23.834, 25, 26.234, 28 and 30 GHz; and 14 channels in the higher (51-59 GHz) V-band frequency band, of which all were used in XPIA: 51.248, 51.76, 52.28, 52.804, 53.336, 53.848, 54.4, 54.94, 55.5, 56.02, 56.66, 57.288, 57.964 and 58.8 GHz. Frequencies in the K-band are more sensitive to water vapor and cloud liquid water, while frequencies in the V-band are sensitive to atmospheric temperature due to the absorption of atmospheric oxygen (Cadeddu et al., 2013). V-band frequencies or channels also can be divided in two categories: the opaque channels, 56.66 GHz and higher, that are more informative in the layer of the atmosphere from the surface to ~1 km AGL, and the transparent channels, 51-56 GHz, that are more informative above 1 km AGL. Both MWRs observed at the zenith and at 15-

Formatted: *Font: 11 pt, Highlight*

Formatted: *Space After: 12 pt, Line spacing: Double, Border: Top: (No border), Bottom: (No border), Left: (No border), Right: (No border), Between : (No border)*

and 165-degree elevation angles in the north-south plane (referred to as oblique elevation scans hereafter; note zenith views have 90-degree elevation ~~angles~~angle). In addition, each MWR was provided with a separate surface sensor to measure pressure, temperature, and relative humidity at the installation level that was ~2.5 m ~~above ground level (AGL).~~ AGL. ~~MWRs are passive devices which record the natural microwave emission in the water vapor and oxygen absorption bands from the atmosphere, providing measurements of the brightness temperatures.~~ Vertical profiles of temperature (T), water vapor density (WVD), and relative humidity (RH) were retrieved in real-time during XPIA every 2-3 minutes using a neural network (NN) approach provided by the manufacturer of the radiometer, Radiometrics (Solheim et al. 1998a, and 1998b; Ware et al., 2003~~NN approach provided by the private manufacturing company Radiometrics (Solheim et al. 1998). The NN used a training dataset based on a 5-year climatology of profiles from radiosondes launched at the Denver International Airport, 35 miles south-east from the XPIA site. NN-based MWR vertical retrieval profiles were obtained using the zenith and an average of two oblique elevation scans, all extending for 58 levels up to 10 km, with nominal vertical levels depending on the height (every 50 m from the surface to 500 m, every 100 m from 500 m to 2 km, and every 250 m from 2 to 10 km, AGL). In this study we make use of the NN zenith and of the NN oblique, where the latter can average out small-scale horizontal inhomogeneities of the atmosphere~~). Although the physical retrieval configurations used in this study do not exactly match the MWR configurations used for NN retrievals, a comparison of both physical and neural network retrievals to the radiosonde temperature data is presented in Appendix A.

__Formatted:__ Space After: 12 pt, Line spacing: Double, Border: Top: (No border), Bottom: (No border), Left: (No border), Right: (No border), Between : (No border)

~~The MWR-CU~~ Both MWRs nominally operated from 9 March to 7 May 2015, ~~while~~although the MWR-NOAA was unavailable between 5-27 April 2015. For the overlapping dates, temperature profiles retrieved from the two MWRs showed very good agreement with less than 0.5 ~~K~~°C bias and 0.994 correlation (Bianco et al., 2017). For this reason, and because the MWR-CU was available for a longer time period, we use only the MWR-CU (hereafter simply called MWR).

Formatted: *Indent: First line: 0.5"*

2.2 Radiosonde measurements

Between 9 March and 7 May 2015, while the MWR was operational, radiosondes were launched by the National Center for Atmospheric Research (NCAR) assisted by several students from the University of Colorado over three selected periods, one each in March, April, and May. There was a total of 59 launches, mostly four times per day, around 14:00, 18:00, 22:00 and 0200 UTC (8:00, 12:00, 16:00 and 20:00 local standard time, LST). All radiosondes were Vaisala RS92. The first 35 launches, between 9-19 March, were done from the visitor center, while the 11 launches, between 15-22 April, and 13 launches, between 1-4 May, were done from the water tank site, ~1000 meters apart (see Lundquist et al., 2017 for a detailed map of the study area). The radiosonde measurements included temperature, dewpoint temperature, and relative humidity, to altitudes usually higher than 10 km AGL, with measurements every few seconds.

Formatted: *Font: Not Bold*

Formatted: *Indent: First line: 0.5"*

2.3 WPR-RASS measurements

Formatted: *Space After: 12 pt, Line spacing: Double, Border: Top: (No border), Bottom: (No border), Left: (No border), Right: (No border), Between : (No border)*

Two NOAA wind profiling radars (WPRs), operating at frequencies of 915-MHz and 449-MHz, were deployed at the visitor center (same location ~~of~~as the MWR) during XPIA. These systems are primarily designed to measure the vertical profile of the horizontal wind vector, but co-located RASS also observe profiles of virtual temperature in the lower atmosphere, with different resolutions and height coverages depending on the WPR. Thus, the RASS associated with the 915-MHz WPR (hereafter referred to as RASS 915) measured virtual temperature from 120 to 1618 m with a vertical resolution of 62 m, and the 449 MHz RASS (hereafter referred to as RASS 449) sampled the boundary layer from 217 to 2001 m with a vertical resolution of 105 m. The maximum height reached by the RASS is a function of both radar frequency and atmospheric conditions (May and Wilczak, 1993), and is usually lower for RASS 915 data, as will be shown later in the analysis.

The RASS data were processed using a radio frequency interference (RFI)-removal algorithm (performed on the RASS spectra), a consensus algorithm (Strauch et al. 1984) performed on the moment data using a 60% consensus threshold, a Weber-Wuertz outlier removal algorithm (Weber et al., 1993) performed on the consensus averages, and a RASS range-correction algorithm (Görsdorf and Lehmann, 2000) using an average relative humidity setting of 50% determined from the available observations.

2.4 BAO data

The BAO 300-m tower was built in 1977 to study the planetary boundary layer (Kaimal and Gaynor 1983). During XPIA, measurements were collected at the surface (2 m) and at six higher levels (50, 100, 150, 200, 250 and 300 m AGL). Each tower level was equipped with 2

Formatted: *Space After: 12 pt, Line spacing: Double, Border: Top: (No border), Bottom: (No border), Left: (No border), Right: (No border), Between : (No border)*

sonic anemometers on orthogonal booms, and one sensor based on a Sensiron SHT75 solid-state sensor to measure temperature and relative humidity with a time resolution of 1 s, and averaged over five minutes.

The observational temperature and water vapor surface data are used from the more accurate observations at the BAO tower 2 m AGL level (Horst~~,~~ et al., 2016), to replace the data measured by the less accurate MWR inline surface sensor.

3. Physical retrievals

~~Other than NN approaches, a~~A physical retrieval (PR) iterative approach can be used to retrieve vertical profiles of thermodynamic properties from the MWR observations (Maahn et al 2020). In this case, using a radiative transfer model, the process starts with a climatologically reasonable value of temperature and water vapor, and is iteratively repeated until the computed brightness temperatures match those observed by the MWR within the uncertainty of the observed brightness temperatures (Rodgers, 2000; Turner and Löhnert, 2014; Maahn et al. 2020).

3.1 Iterative retrieval technique

For this study, the ~~physical retrieval (PR)~~PR uses a microwave radiative transfer model, MonoRTM (Clough et al., 2005), which is fully functional for the microwave region and was intensively evaluated previously on MWR measurements (Payne et al. 2008; 2011). We start with the state vector $\mathbf{X_a} = [\mathbf{T}, \mathbf{Q}, \mathrm{LWP}]^T$, where superscript T denotes transpose. **T** (K) and **Q**

Formatted: *Outline numbered + Level: 1 + Numbering Style: 1, 2, 3, … + Start at: 1 + Alignment: Left + Aligned at: 0.25" + Indent at: 0.5"*

Formatted: *Space Before: 0 pt, After: 0 pt*

Formatted: *Space Before: 0 pt, After: 0 pt, Border: Top: (No border), Bottom: (No border), Left: (No border), Right: (No border), Between : (No border)*

Formatted: *Space After: 12 pt, Line spacing: Double, Border: Top: (No border), Bottom: (No border), Left: (No border), Right: (No border), Between : (No border)*

(g/kg) are temperature and water vapor mixing ratio profiles at 55 vertical levels from the surface up to 17 km, with the distance between the levels increasing exponentially-like with height. LWP is the liquid water path in (g/m^2) that measures the integrated content of liquid water in the entire vertical column above the MWR, and is a scalar. For this study we have $\mathbf{X_a}$ with dimensions equal to 111 x 1 (two vectors **T** and **Q** with 55 levels each, and LWP). ~~-~~We are using the retrieval framework of Turner and Blumberg (2019), but only using MWR data (no spectral infrared) and will augment the retrieval to include RASS profiles of Tv.

The observation vector **Y** from the beginning includes temperature and water vapor mixing ratio measured at the surface, and ~~brightness temperature (~~**Tb**~~)~~ measured by the MWR. The MonoRTM model **F** is used as the forward model ~~to estimate the observation vector Y~~ from the current state vector **X**, ~~from~~ Eq. ~~(1),~~(1), and is then compared to the observation vector **Y**, iterating until the difference between **F(X)** and **Y** is small within a specified uncertainty~~:~~.

$$\cancel{X_{n+1} = X_a + (S_a^{-1} + K^T S_\varepsilon^{-1} K)^{-1} K^T S_\varepsilon^{-1} [Y - F(X_n) + K(X_n - X_a)]} \quad \cancel{(1)}$$

$$\boldsymbol{X}_{n+1} = \boldsymbol{X}_n + (\boldsymbol{S}_a^{-1} + \boldsymbol{K}^T \boldsymbol{S}_\varepsilon^{-1} \boldsymbol{K})^{-1} \boldsymbol{K}^T \boldsymbol{S}_\varepsilon^{-1} [Y - \boldsymbol{F}(\boldsymbol{X}_n) + \boldsymbol{K}(\boldsymbol{X}_n - \boldsymbol{X}_a)] \quad (1)$$

with~~:~~

$$\boldsymbol{X}_a = \begin{bmatrix} \boldsymbol{T} \\ \boldsymbol{Q} \\ L \end{bmatrix} \qquad \boldsymbol{S}_a = \begin{bmatrix} \boldsymbol{\sigma}^2_{TT} & \boldsymbol{\sigma}^2_{TQ} & 0 \\ \boldsymbol{\sigma}^2_{QT} & \boldsymbol{\sigma}^2_{QQ} & 0 \\ 0 & 0 & \sigma^2_L \end{bmatrix} \quad \boldsymbol{K}_{ij} = \frac{\partial \boldsymbol{F}_i}{\partial \boldsymbol{X}_j}$$

$$\boldsymbol{S}_\varepsilon = \begin{bmatrix} \sigma^2_{T\,sfc} & 0 & 0 & 0 & 0 \\ 0 & \sigma^2_{Q\,sfc} & 0 & 0 & 0 \\ 0 & 0 & \boldsymbol{\sigma}^2_{Tb_{zenith}} & 0 & 0 \\ 0 & 0 & 0 & \boldsymbol{\sigma}^2_{Tb_{zenith+oblique}} & 0 \\ 0 & 0 & 0 & 0 & \boldsymbol{\sigma}^2_{Tv_{RASS915(449)}} \end{bmatrix}$$

① ② 3 or 4

Formatted: *Indent: First line: 0"*

Formatted: *Font: 11 pt*

Formatted: *Font: Not Bold*

Formatted: *Space After: 12 pt, Line spacing: Double, Border: Top: (No border), Bottom: (No border), Left: (No border), Right: (No border), Between : (No border)*

$$\boldsymbol{X_a} = \begin{bmatrix} \boldsymbol{T} \\ \boldsymbol{Q} \\ LWP \end{bmatrix} \quad \boldsymbol{S_a} = \begin{bmatrix} \boldsymbol{\sigma^2_{TT}} & \boldsymbol{\sigma^2_{TQ}} & 0 \\ \boldsymbol{\sigma^2_{QT}} & \boldsymbol{\sigma^2_{QQ}} & 0 \\ 0 & 0 & \sigma^2_{LWP} \end{bmatrix} \qquad \boldsymbol{K_{ij}} = \frac{\partial \boldsymbol{F}_i}{\partial \boldsymbol{X}_j}$$

$$\boldsymbol{S_\varepsilon} = \begin{bmatrix} \sigma^2_{Tsfc} & 0 & 0 & 0 \\ 0 & \sigma^2_{Qsfc} & 0 & 0 \\ 0 & 0 & \boldsymbol{\sigma^2_{Tb_{zenith}}} \ (1) \ \boldsymbol{or} \ \boldsymbol{\sigma^2_{Tb_{zenith+oblique\ avrg}}} \ (2) & 0 \\ 0 & 0 & 0 & \boldsymbol{\sigma^2_{Tv_{RASS915(449)}}} \ (3 \text{ or } 4) \end{bmatrix}$$

where i and j in the K_{ij} definition mark channel and vertical level respectively, and **Y**, depending on the configuration used, being equal to:

$$\boldsymbol{Y_1} = \begin{bmatrix} T_{sfc} \\ Q_{sfc} \\ \boldsymbol{Tb_{zenith}} \end{bmatrix} \qquad \boldsymbol{Y_2} = \begin{bmatrix} T_{sfc} \\ Q_{sfc} \\ \boldsymbol{Tb_{zenith}} \\ \boldsymbol{Tb_{zenith+oblique}} \end{bmatrix}$$

$$\boldsymbol{Y_3} = \begin{bmatrix} T_{sfc} \\ Q_{sfc} \\ \boldsymbol{Tb_{zenith}} \\ \boldsymbol{Tb_{zenith+oblique}} \\ \boldsymbol{Tv_{RASS915}} \end{bmatrix} \qquad \boldsymbol{Y_4} = \begin{bmatrix} T_{sfc} \\ Q_{sfc} \\ \boldsymbol{Tb_{zenith}} \\ \boldsymbol{Tb_{zenith+oblique}} \\ \boldsymbol{Tv_{RASS449}} \end{bmatrix}$$

$$\boldsymbol{Y_1} = \begin{bmatrix} T_{sfc} \\ Q_{sfc} \\ \boldsymbol{Tb_{zenith}} \end{bmatrix} \qquad \boldsymbol{Y_2} = \begin{bmatrix} T_{sfc} \\ Q_{sfc} \\ \boldsymbol{Tb_{zenith+oblique\ avrg}} \end{bmatrix}$$

$$\boldsymbol{Y_3} = \begin{bmatrix} T_{sfc} \\ Q_{sfc} \\ \boldsymbol{Tb_{zenith+oblique\ avrg}} \\ \boldsymbol{Tv_{RASS915}} \end{bmatrix} \qquad \boldsymbol{Y_4} = \begin{bmatrix} T_{sfc} \\ Q_{sfc} \\ \boldsymbol{Tb_{zenith+oblique\ avrg}} \\ \boldsymbol{Tv_{RASS449}} \end{bmatrix}$$

Formatted: *Indent: First line: 0"*

Formatted: *Space After: 12 pt, Line spacing: Double, Border: Top: (No border), Bottom: (No border), Left: (No border), Right: (No border), Between : (No border)*

The superscripts T and -1 in (1) indicate transpose or inverse matrix, respectively. Also, vectors and matrices are shown in bold.~~-~~ Note that we are including the 2-m surface-level observations of temperature and water vapor mixing ratio (Tsfc and Qsfc, respectively) as part of the observation vector $\mathbf{Y}$, and thus the uncertainties in these observations are included in $\mathbf{S}_{\varepsilon}$.

The first guess of the state vector $\mathbf{X}$, $\mathbf{X}_1$ in Eq. (1), is set to be equal to the mean state vector of climatological estimates, or a "prior" vector $\mathbf{X}_a$, which is calculated independently for each month of the year from climatological sounding profiles (using 10 years of data) in the Denver area.

$\mathbf{S}_a$ is the covariance matrix of the "prior" vector that includes not only temperature or water vapor variances but also the covariances between them. Using 3,000 radiosondes launched by the NWS in Denver, we interpolated each radiosonde profile to the vertical levels used in the retrieval, after which we computed the covariance of temperature and temperature, temperature and humidity, and humidity and humidity for different levels. $\mathbf{K}$ is the Jacobian matrix, computed using finite differences by perturbing the elements of $\mathbf{X}$ and rerunning the radiative transfer model.

We start with four configurations for the observational vector $\mathbf{Y}$ ($\mathbf{Y}_1$, $\mathbf{Y}_2$, $\mathbf{Y}_3$, and $\mathbf{Y}_4$). The MWR provides ~~the~~ **Tb** measurements ~~in all schemes,~~ from 22 channels from the zenith scan for the zenith only ~~in~~ configuration ($\mathbf{Y}_1$ ~~(~~, which also includes the 2-m in-situ observations of temperature and humidity), ~~and~~while when using the zenith ~~and~~plus oblique ~~in~~ Tb inputs ($\mathbf{Y}_2$, $\mathbf{Y}_3$, and $\mathbf{Y}_4$, also including the 2-m in-situ observations of temperature and humidity) the same 22 channels were used from the zenith scans together with only the four opaque channels (56.66, 57.288, 57.964 and 58.8 GHz) from the oblique scans. Using additional measurements

Formatted: *Font: Bold*

Formatted: *Indent: First line: 0.5"*

Formatted: *Font: Bold*

Formatted: *Font: Bold*

Formatted: *Space After: 12 pt, Line spacing: Double, Border: Top: (No border), Bottom: (No border), Left: (No border), Right: (No border), Between : (No border)*

from the co-located radar systems with RASS, we may further expand the observational vector with either RASS 915 (**Y**$_3$) or RASS 449 (**Y**$_4$) virtual temperature observations. The covariance matrix of the observed data, **S**$_\varepsilon$, depends on the chosen **Y**$_i$ as it is highlighted by the red numbers in the matrix description, with increasing dimensions from **Y**$_1$ to **Y**$_2$ and additional increasing dimensions to **Y**$_3$ ~~and~~or **Y**$_4$ through the multi-level measurements of the RASS (Turner and Blumberg, 2019). Table 1 summarizes the observational information included in these four different configurations of the PR.

	T_{sfc}	Q_{sfc}	Tb_{zenith}	~~$Tb_{zenith-oblique}$~~ $Tb_{oblique\_avrg}$	$Tv_{RASS915}$	$Tv_{RASS449}$
***Y*$_1$** = *MWRz*	*X*	*X*	*X*			
***Y*$_2$** = *MWRzo*	*X*	*X*	*X*	*X*		
***Y*$_3$** = *MWRzo915*	*X*	*X*	*X*	*X*	*X*	
***Y*$_4$** = *MWRzo449*	*X*	*X*	*X*	*X*		*X*

*Table 1. Four PR configurations corresponding to the four observational **Y**$_i$ vectors in Eq. (1).*

The uncertainty in the MWR Tb observations was set to the standard deviation from a detrended time-series analysis for each channel during cloud-free periods, which is described in detail in Section 3.2. The derived uncertainties ranged from 0.3 K to 0.4 K in the 22 to 30 GHz

Formatted: *Font: 14 pt, Italic*

Formatted: *Space After: 8 pt, Line spacing: Multiple 1.08 li*

Formatted: *Font: 11 pt, Italic*

Formatted: *Indent: First line: 0", Space After: 8 pt, Line spacing: Multiple 1.08 li*

Formatted Table

Formatted: *Font: 14 pt, Italic*

Formatted: *Font: 14 pt, Italic*

Formatted: *Space After: 8 pt, Line spacing: Multiple 1.08 li*

Formatted: *Font: 14 pt, Italic*

Formatted: *Space After: 8 pt, Line spacing: Multiple 1.08 li*

Formatted: *Font: 14 pt, Italic*

Formatted: *Space After: 8 pt, Line spacing: Multiple 1.08 li*

Formatted: *Font: 14 pt, Italic*

Formatted: *Space After: 8 pt, Line spacing: Multiple 1.08 li*

Formatted: *Space After: 12 pt, Line spacing: Double, Border: Top: (No border), Bottom: (No border), Left: (No border), Right: (No border), Between : (No border)*

channels, and 0.4 to 0.7 K in the 52 to 60 GHz channels. We ~~assume~~assumed that there ~~is~~was no ~~covariance~~correlated error between the different ~~instruments~~MWR channels.

For the RASS, collocated RASS and radiosonde profiles were compared and the standard deviation of the differences in Tv were determined as ~~well as~~a function of the radar's signal-to-noise ratio (SNR). This relationship resulted in uncertainties that ranged from 0.8 K at high SNR values to 1.5 K at low SNR values. Again, we assumed that there was no correlated error between different ~~channels (MWR) or height levels (RASS) of each instrument, therefore this~~RASS heights. Following all these assumptions, the covariance matrix $\mathbf{S}_\varepsilon$ is diagonal.

The Jacobian matrix, **K**, has dimensions m x 111, where m is the length of the vector $\mathbf{Y}_i$, therefore its ~~dimensions increase~~dimension increases correspondingly with the inclusion of more observational data. **K** makes the "connection" between the state vector and the observational data and should be calculated at every iteration.

3.2 ~~Bias~~Physical retrieval bias-correction and temperature profiles

Observational errors propagate through the retrieval into the derived profiles (i.e. the bias of the observed data will contribute to a bias in the retrievals.) For that, retrieval uncertainties in Eq. (1) from $\mathbf{Y} = \mathbf{Y}_1$ or $\mathbf{Y}_2$ derive only from uncertainties in surface and MWR data, while retrieval uncertainties from $\mathbf{Y} = \mathbf{Y}_3$ or $\mathbf{Y}_4$ are coming from uncertainties in surface, MWR, and RASS measurements.

While the bias of the retrieval depends on both the sensitivity of the forward model and the observational ~~uncertainty~~systematic offset, we can try to eliminate, or at least to reduce, the systematic error in the MWR observations. To this aim, we first looked for clear sky days (to

Formatted: *Space After: 12 pt, Line spacing: Double, Border: Top: (No border), Bottom: (No border), Left: (No border), Right: (No border), Between : (No border)*

reduce the degrees of freedom associated with clouds) during the period of the measurements. One method to identify clear-sky times is to use ~~brightness temperature~~ Tb observations in the 30 GHz liquid water ~~vapor~~ sensitive channel. The random uncertainty in ~~brightness temperature was~~ Tb is calculated as ~~its~~an average of the Tb standard deviation ~~during clear sky times and for this channel is approximately 0.3 K (but during periods with liquid-bearing clouds overhead,~~ in a one-hour sliding window through all data points of a day. (It also could be computed as the standard deviation of the ~~30 GHz Tb is markedly higher than this threshold due~~difference between Tb and the smoothed Tb to ~~the non-homogeneous nature of clouds and thus their contribution to the downwelling microwave radiance).~~eliminate daily temperature variability.) Four clear-sky days ~~were selected,~~have been chosen using a criterion of 0.3 K uncertainty in the 30 GHz channel: March 10 and 30, and April 13 and 29~~.~~, 2015. During periods with liquid-bearing clouds overhead, this criterion is markedly higher (more than 0.7 K) and much higher for the rainy periods (> 4 K). While those calculations were applied on a daily basis, it is important to mention that the days are not uniform in terms of cloudiness or rain. Therefore, we used the data for 2-3 hours around the time of radiosonde launches to determine to which category a particular radiosonde profile belongs, clear-sky, cloudy or rain. In this way, we found that from 58 radiosonde launches used in our statistical analysis, 41 belong to the clear-sky category, 12 - to cloudy but non-precipitating conditions, and 5 - to rainy periods. For the four chosen clear-sky days not only were the daily uncertainties of 30 GHz Tb below 0.3 K, but both sets of uncertainties described above were extremely similar with the averaged difference less than 0.05 K.

Formatted: *Space After: 12 pt, Line spacing: Double, Border: Top: (No border), Bottom: (No border), Left: (No border), Right: (No border), Between : (No border)*

The bias was ~~then~~ computed ~~on all~~for each of the 22 channels as the averaged difference between the observed Tb from the MWR zenith observations, and the forward model calculation applied to the prior, over these selected clear-sky days, and then subsequently removed from all ~~measurements~~of the observations. We compute the bias in the bias-correction procedure only from the zenith scans, assuming that the same bias is suitable for other scans. Also, we assume that the true bias is an offset that is nearly independent of the scene, so that the sensitivity to the scene (e.g., clear or cloudy, zenith or off-zenith) is small. To investigate that, we eliminated the radiosondes launched during rainy periods (5 out of 58 cases) and found that the average temperature profiles were very little different than when all radiosonde profiles were used, with the maximum bias and RMSE absolute differences 0.12 K and 0.11 K respectively up to 5 km AGL. Fig. 1 shows the results of the bias-correction for the four chosen clear-sky days. The green lines on this figure indicate the MWR random errors ~~at each frequency calculated as the standard deviation of Tb averaged over one-hour sliding window~~; these are 0.3-0.4 K for K-band channels and 0.~~6~~4-0.7 K for V-band channels.

Formatted: Font color: Black

Formatted

Formatted: Space After: 12 pt, Line spacing: Double, Border: Top: (No border), Bottom: (No border), Left: (No border), Right: (No border), Between : (No border)

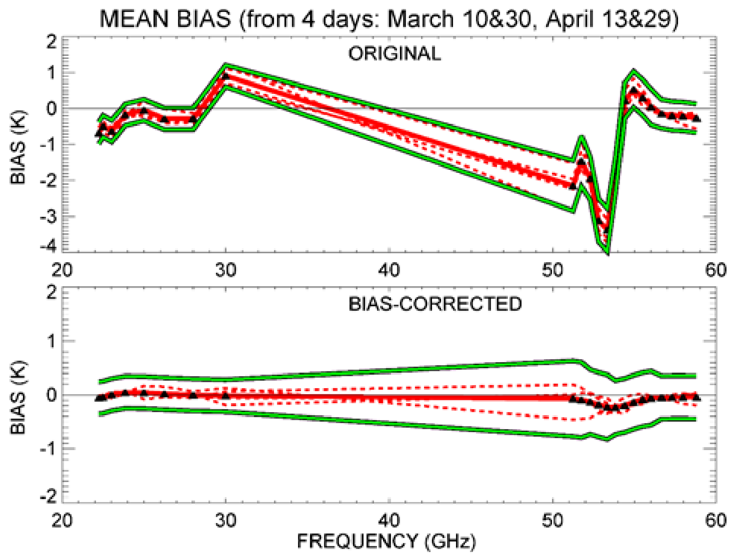

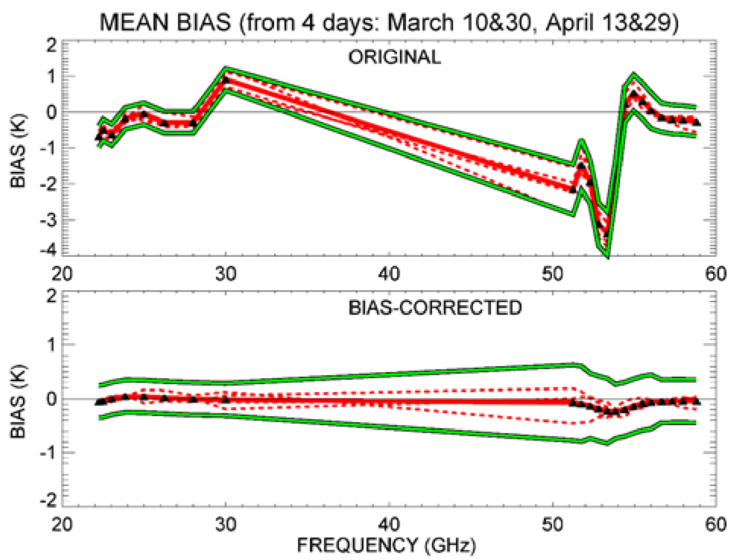

Formatted: *Space After: 12 pt, Line spacing: Double, Border: Top: (No border), Bottom: (No border), Left: (No border), Right: (No border), Between : (No border)*

Fig.1. Bias for the four chosen clear-sky days (red-dashed lines) and their mean (red solid line) for the original observations in the top panel, and for the bias-corrected data in the bottom panel. Green lines are the uncertainty boundaries around the mean bias. Frequencies used in the PR algorithm are marked with black triangles in both panels.

Formatted: *Indent: First line: 0"*

~~This bias correction was applied to the brightness temperature used in the PR approach; however, the NN retrievals used the uncorrected brightness temperature, since it was non-trivial for us to reprocess those retrievals.~~

The retrieved profiles of the four different PR configurations presented in Table 1 (MWRz, MWRzo, MWRzo915, MWRzo449) were compared to the radiosonde profiles~~, as well as to the NN retrievals.~~. BAO tower temperature and mixing ratio data at the seven available levels were used as an additional validation dataset, without any interpolation.

To compare radiosonde observations against the PR ~~and NN retrieved~~ profiles, all these profiles were interpolated vertically to the same PR heights, and PR~~ and NN~~ profiles were averaged in the time window between 15 minutes before and 15 minutes after each radiosonde launch. Since the radiosonde ascends quite quickly in the lowest kilometers of the atmosphere (~15-20 min to reach 5 km), we estimated that the 30-minute temporal window is representative of the same volume of the atmosphere measured by the radiosonde.

An example of the different temperature retrievals and their relative performance, data obtained on 17 March 2015 at 2200 UTC is presented in Fig. 2. Temperature profiles up to 2 km

Formatted: *Space After: 12 pt, Line spacing: Double, Border: Top: (No border), Bottom: (No border), Left: (No border), Right: (No border), Between : (No border)*

AGL from the four PR configurations (MWRz, MWRzo, MWRzo915, MWRzo449) are compared to the radiosonde data in red~~,~~ and to the BAO measurements in blue squares~~, and to the NN profiles (NN zenith in beige, and NN oblique in green).~~. The MWRz and MWRzo profiles~~, as well as those from the NNs,~~ are very smooth and depart quite substantially from the radiosonde measurements, being unable to reproduce the more detailed structure of the atmospheric temperature profile measured by the radiosonde, while the MWRzo449 profile (in light-blue) demonstrates a better agreement with both the radiosonde and BAO measurements (blue squares). Note that all four of the PRs match the BAO observations reasonably well~~, while the NN retrievals are warm-biased.~~ . The MWRzo915 profile (in magenta) also tries to follow the elevated temperature inversion observed by the radiosonde, successfully only in the lower part of the atmosphere (below 1 km AGL) where RASS 915 measurements are available. This behavior will be also addressed in the following section and in the statistical analysis presented later in the manuscript.

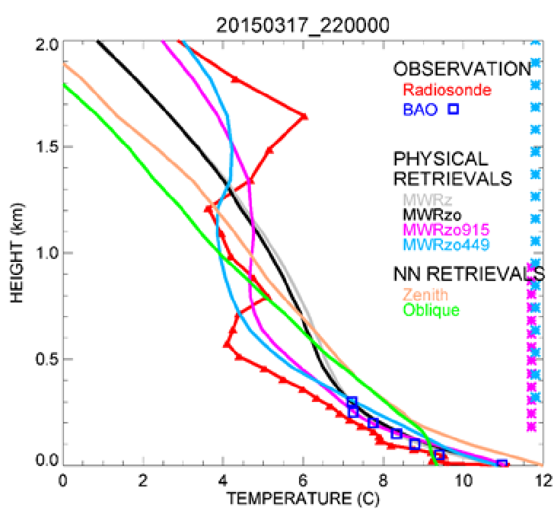

Formatted: *Space After: 12 pt, Line spacing: Double, Border: Top: (No border), Bottom: (No border), Left: (No border), Right: (No border), Between : (No border)*

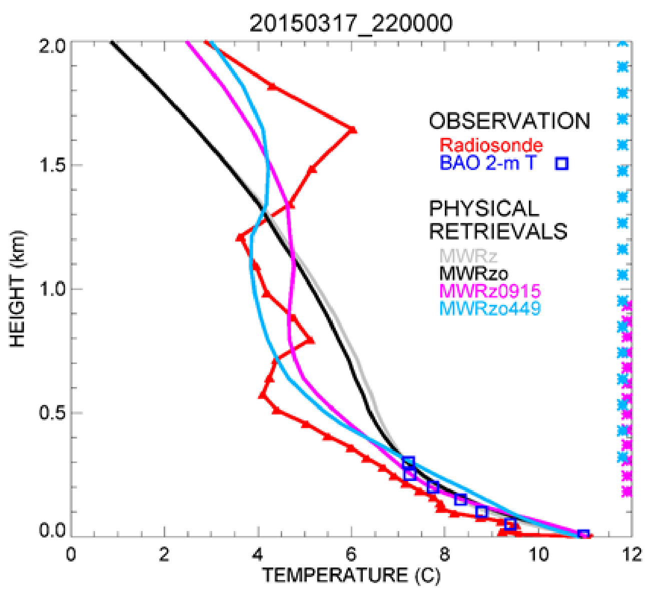

Fig. 2. Temperature profiles obtained by the four PR configurations: MWRz in gray, MWRzo in black, MWRzo915 in magenta, and MWRzo449 in light-blue~~; NN retrievals: NN zenith in beige, and NN averaged oblique in green.~~. These retrievals are compared to radiosonde measurements, in red, and BAO tower observations, in blue squares. The heights with available RASS virtual temperature measurements (RASS 915 in magenta and RASS 449 in light-blue), are marked by the asterisks on the right Y-axis.

3.3 Averaging kernel

The averaging kernel, **Akernel** (Masiello et al., 2012, Turner and Löhnert, 2014) from Eq. (1) can be calculated as:

$$\boldsymbol{Akernel = B^{-1}\, K^{T}\, S_{\varepsilon}^{-1}\, K} \qquad (2)$$

Formatted: *Space After: 12 pt, Line spacing: Double, Border: Top: (No border), Bottom: (No border), Left: (No border), Right: (No border), Between : (No border)*

where:

$$B = S_a^{-1} + K^T S_\varepsilon^{-1} K$$

Both matrices, **Akernel** and **B**, have dimensions 111 x 111 in our configuration. The **Akernel** ~~matrix has~~ provides useful information about the calculated retrievals, such as vertical resolution and degrees of freedom for signal at each level. Thus, the rows of **Akernel** provide the smoothing functions that have to be applied to the retrievals (Rodgers, 2000) to help minimize the vertical representativeness error in the comparison between the various retrievals and the radiosonde profiles due to very different vertical resolutions of these profiles.

Using the averaging kernel, the smoothed radiosonde observed profiles will be therefore computed as:

$$X_{smoothed\_sonde} = Akernel\ (X_{sonde} - X_a) + X_a \qquad (3)$$

The **Akernel** in Eq. (2) depends on the retrieval parameters (e.g., which datasets are used in the **Y** vector, the values assumed in the observation covariance matrix $\mathbf{S_\varepsilon}$, and the sensitivity of the forward model (i.e., its Jacobian), etc.), so for our four PR configurations it is possible to calculate four different kernels: **A_MWRz, A_MWRzo, A_MWRzo915 and A_MWRzo449**, respectively.

While the top left corner of the **Akernel** matrix (1:55, 1:55) is devoted to temperature, and it will be called **AT_MWR** hereafter, the next (56:110, 56:110) elements are devoted to water vapor mixing ratio, and will be called **AQ_MWR**.

Formatted: *Font: Bold*

Formatted: *Space After: 12 pt, Line spacing: Double, Border: Top: (No border), Bottom: (No border), Left: (No border), Right: (No border), Between : (No border)*

For each of the four **Akernels**, a smoothed radiosonde profile can be computed for each radiosonde profile using Eq. (3). In the presence of temperature inversions or other particular structures in the atmosphere these smoothed profiles can be quite different from each other and also from the original unsmoothed radiosonde profile.

Therefore, in the statistical analysis presented later in the manuscript (in section 4.2), mean bias, root mean square error (RMSE), and Pearson correlation coefficients will be computed between the MWR's retrievals and both the unsmoothed and smoothed radiosonde profiles, where the latter were computed using their respective **Akernels**. Additional observational data help to resolve the atmospheric structure in more detail, therefore we would expect to obtain better statistical evaluations from the configurations including additional RASS observations compared to the runs without RASS data.

The improvement in the retrieved temperature profiles presented in Fig. 2 obtained using additional RASS data can be explained and clearly shown by the **ATkernel** itself. Figure 3 includes the temperature profiles of the radiosonde (unsmoothed and **ATkernel**'s smoothed) and PRs of MWRzo and MWRzo449 (panel a), and the **ATkernels** corresponding to these PRs in the color plots in the middle of the figure (panels b and c). These color plots are a schematic visualization of the 37 x 37 top left corner of the **ATkernel** matrix that illustrates the part of the **ATkernel** up to 3 km, for reference. Dash lines mark the 2 km vertical level.

The rows of the **ATkernel** provide a measure of the retrieval smoothing as a function of altitude, so the full-width half maximum of each **ATkernel** row estimates the vertical resolution of the retrieved solution at each vertical level (Merrelli and Turner, 2012). These plots of

Formatted: *Space After: 12 pt, Line spacing: Double, Border: Top: (No border), Bottom: (No border), Left: (No border), Right: (No border), Between : (No border)*

temperature vertical resolution ~~vs~~versus height for MWRzo and MWRzo449 are included in Figure 3, panel d, for the same case presented in Fig. 2. Comparison of **ATkernel** color plots and vertical resolution plots of MWRzo vs MWRzo449 shows that additional observations from the RASS 449 significantly reduces the spread around the main diagonal from ~200m up to 2 km (in the layer of the atmosphere where RASS 449 measurements are available), thereby improving the vertical resolution of the retrievals (as clearly visible in panel d).

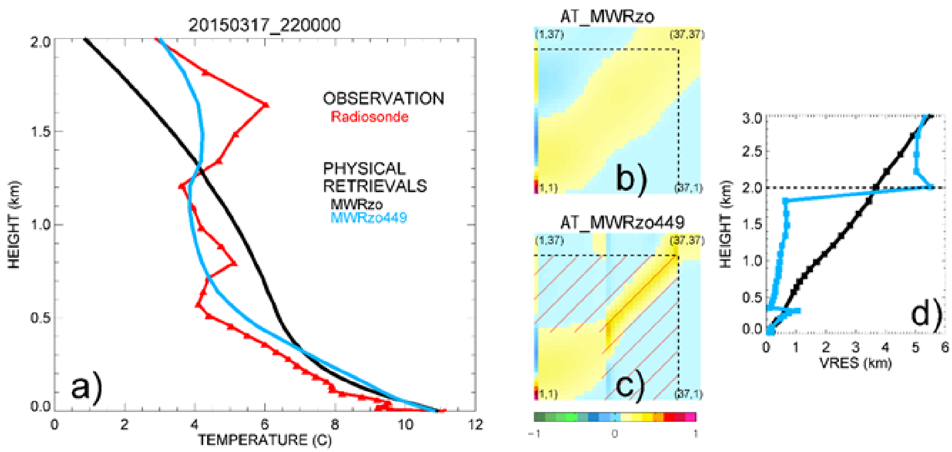

Formatted: *Space After: 12 pt, Line spacing: Double, Border: Top: (No border), Bottom: (No border), Left: (No border), Right: (No border), Between : (No border)*

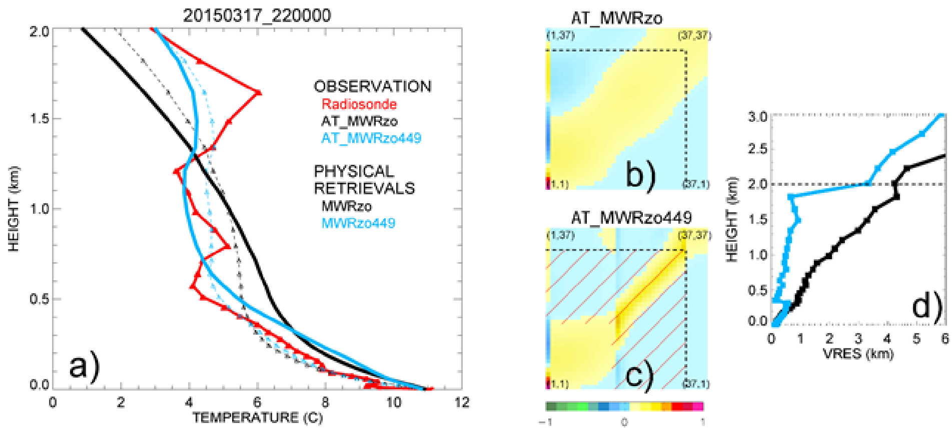

Fig. 3. Panel a: observed temperature profiles from radiosonde, in red, from ATkernels smoothed radiosonde, ***AT_MWRzo*** *in dashed black, and* ***AT_MWRzo449*** *in dashed light-blue; PRs from MWRzo PR in black, and from MWRzo449 PR in light-blue. Middle colored panels: 37x37 levels (surface to 3 km) of the Akernel matrix for temperature, b)* ***AT_MWRzo*** *and c)* ***AT_MWRzo449****. Right panel d: vertical resolution (VRES) as a function of the height for the MWRzo PR (black), and for the MWRzo449 PR (light-blue). ~~Dash~~Dashed lines on plots b)-d) mark 2 km AGL. Hatched area on panel c~~)~~ marks the RASS measurement heights.*

4. Results

PR~~ and NN retrieved~~ profiles have been evaluated against radiosonde observations. For additional verification, radiosonde data from 59 launches taken between 9 March and 4 May 2015 were first of all compared to the BAO tower measurements, up to 300 m AGL. These observed data sets match very well, with a correlation coefficient of 0.99 and a standard

Formatted: Outline numbered + Level: 1 + Numbering Style: 1, 2, 3, … + Start at: 1 + Alignment: Left + Aligned at: 0.25" + Indent at: 0.5"

Formatted: Space After: 12 pt, Line spacing: Double, Border: Top: (No border), Bottom: (No border), Left: (No border), Right: (No border), Between : (No border)

deviation of ~0.7 ~~°K.~~ °C. However, one radiosonde profile showed a large bias (> 5 ~~°K~~°C) against all seven levels of BAO temperature measurements and against all PRs~~ and NNs~~, therefore we decided to exclude this particular radiosonde profile from the statistical calculations.

4.1 ~~PRs~~Physical retrieval statistical analysis from Akernel

To complete the analyses on the **ATkernel** changes and dependencies from different types of observational data used in the PRs, the **ATkernels**, averaged over all radiosonde events, are shown in Fig. 4, panels a-d, for the four PR configurations of Table 1, in the same way as shown in Fig. 3, b-c. A clearly visible gradual narrowing of the spread around the main diagonal is obtained by the usage of the additional observations, from MWR zenith only (panel a), to MWR zenith-oblique (panel b), to the larger impact obtained by the usage of RASS 915 (panel c) and RASS 449 (panel d) data.

Other statistically important features to analyze in the PRs, besides vertical resolution, are the retrieval uncertainty, and the degree of freedom for signal (DFS). These three features are also shown in Fig.4, panels e-g, at each of the heights of the retrieved solution, up to 3 km AGL, and averaged over all radiosonde events. While the vertical resolution (panel e) shows the width of the atmosphere layer used for each retrieval height (the vertical resolution is computed as the full-width half-maximum (FWHM; Maddy and Barnet, 2008) value of the averaging kernel), the uncertainty (panel f) gives a measure of the retrieval correctness (computed by propagating the uncertainty of the observations and the sensitivity of the forward model), and the DFS (panel g) is a measure of the number of independent pieces of

__Formatted:__ Space After: 12 pt, Line spacing: Double, Border: Top: (No border), Bottom: (No border), Left: (No border), Right: (No border), Between : (No border)

information used in the retrieved solution. For example, at the 1 km AGL level the vertical resolution of MWRzo449 equals 0.5 km, i.e. information from +/- 0.5 km around the retrieval height are considered in the retrieval, while all other retrievals use the information from +/- 2 km. Also, the uncertainty of the MWRzo449 retrieval up to ~~1km~~1 km AGL is around 0.5 ~~°K~~°C while the other retrievals have higher uncertainties of up to 1 ~~°K~~°C. The higher accuracy of the MWRzo449 retrievals is because they use more observational information compared to the other retrieval configurations.

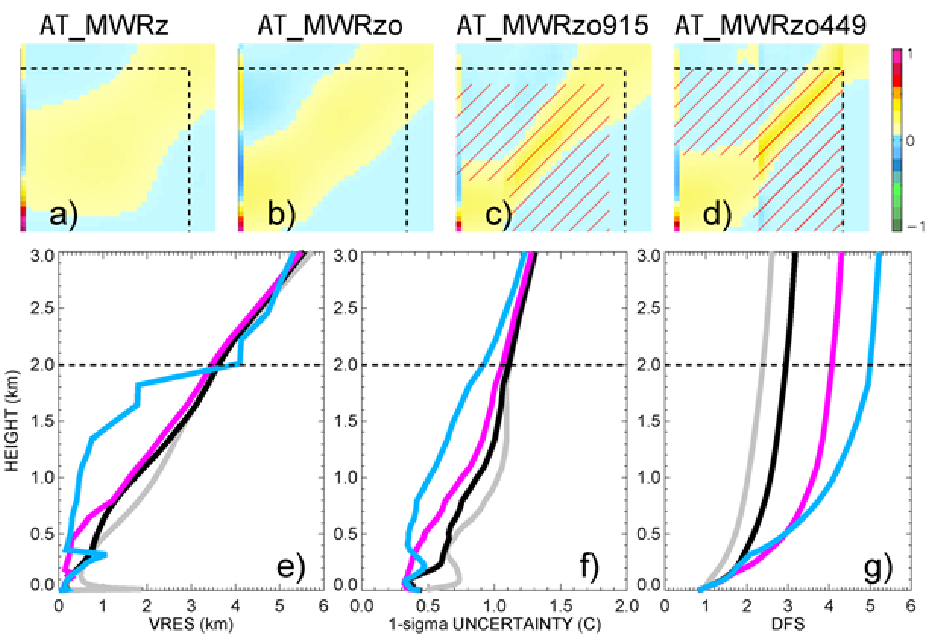

Formatted: *Space After: 12 pt, Line spacing: Double, Border: Top: (No border), Bottom: (No border), Left: (No border), Right: (No border), Between : (No border)*

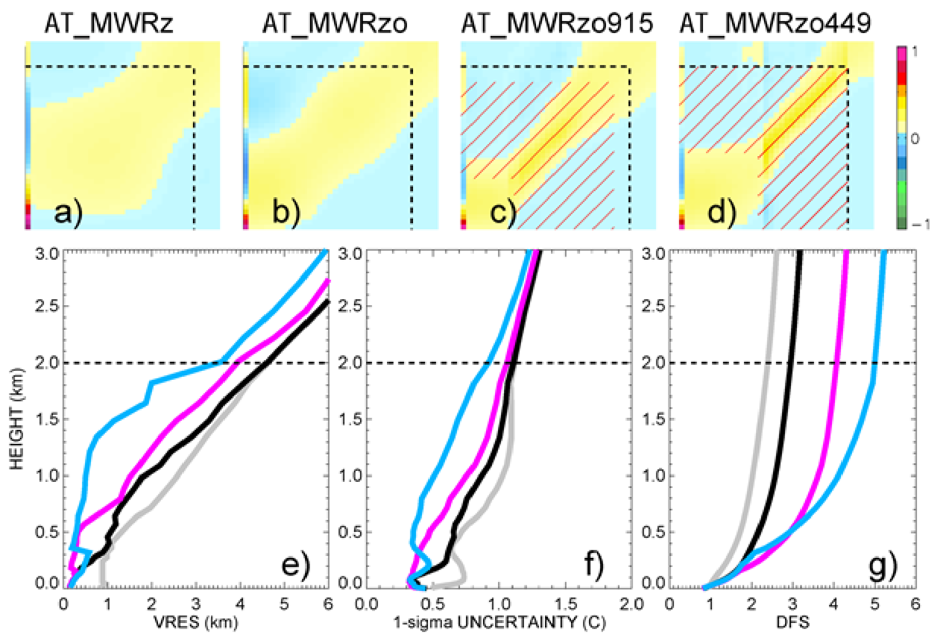

*Fig. 4. Top four-color images: **ATkernels** for MWRz (panel a), MWRzo (panel b), MWRzo915 (panel c) and MWRzo449 (panel d), averaged over all radiosonde events. Hatched area on panels c) and d) marks the RASS measurement heights. Bottom three panels from left to right: vertical resolution (VRES) in km (panel e), one-sigma uncertainty derived from the posterior covariance matrix in °C (panel f), and cumulative Degree of Freedom (DFS, panel g) as a function of height for temperature, averaged over all radiosonde events (MWRz is in gray, MWRzo is in black, MWRzo915 is in magenta, and MWRzo449 is in light-blue). ~~Dash~~Dashed lines mark 2 km AGL on all panels.*

***Formatted:** Space After: 12 pt, Line spacing: Double, Border: Top: (No border), Bottom: (No border), Left: (No border), Right: (No border), Between : (No border)*

The improvements from MWRz (in gray) to MWRzo (in black), then to MWRzo915 (in magenta), and finally to MWRzo449 (in light-blue) are visible in all three panels (Fig 4 e-g), whereas MWRzo449 has the best statistical measures compared to the other PRs, particularly below 2 km AGL, where RASS 449 measurements are available. Finally, it is interesting that below 200 m AGL the MWRzo915 has slightly better statistics compared to the MWRzo449, as could be expected due to the first available height of the RASS 915 being lower (120 m AGL) than the first available height for the RASS 449 (217 m AGL) and due to the finer vertical resolution of the 915-MHz RASS. This suggests that if additional observations were available in the lowest several 100 m ~~layer~~ of the atmosphere where RASS measurements are not available, improvements might be even better closer to the surface, where temperature inversions, if present, are sometimes difficult to retrieve correctly.

As a matter of fact, we found several cases during XPIA when the temperature profile exhibits inversions, with the lowest happening in the surface layer. Figure 5a shows one of the most complex cases, with several temperature inversions visible in the temperature profile from the radiosonde (red line), in the temperature measurements from the BAO tower (blue squares), and in the virtual temperature measured by the RASS 449 (light blue triangles). We note that the virtual temperature profile is in close agreement with the temperature measured by radiosonde. Generally, the moisture contribution to the virtual temperature is less than a degree K, decreasing substantially for dryer air. Among the PR profiles, the PRs including RASS data show better agreement with the radiosonde in the atmospheric layer where RASS measurements are available, as ~~was already~~ shown in Fig. 2 for a different date. Unfortunately,

Formatted: *Space After: 12 pt, Line spacing: Double, Border: Top: (No border), Bottom: (No border), Left: (No border), Right: (No border), Between : (No border)*

this better performance is not visible below the first available RASS measurement, i.e. from the surface up to ~200m AGL, where the PRs with additional RASS data have the largest positive bias compared to both radiosonde and BAO data in this layer. We ~~believe~~found that the MWR data, especially those from the oblique scans, in this case have a bias in the observed brightness temperatures that propagates through the retrieval calculations, and including other observational data is not enough to correct it in the layer between the surface data and the first available RASS measurement.

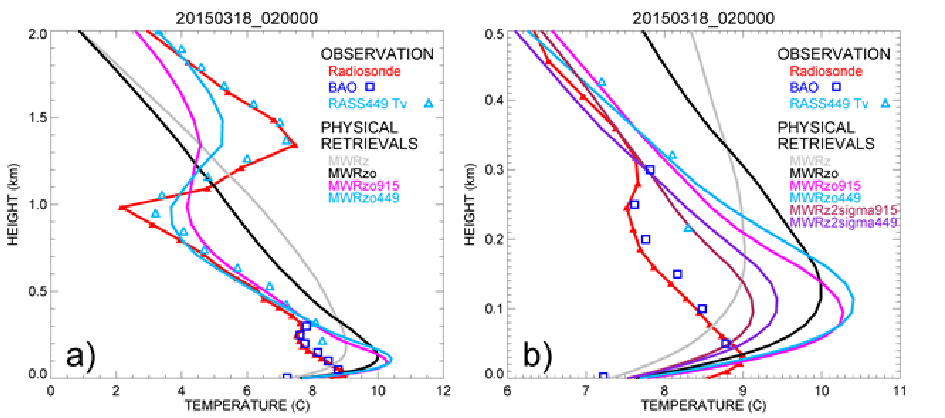

Formatted: Space After: 12 pt, Line spacing: Double, Border: Top: (No border), Bottom: (No border), Left: (No border), Right: (No border), Between : (No border)

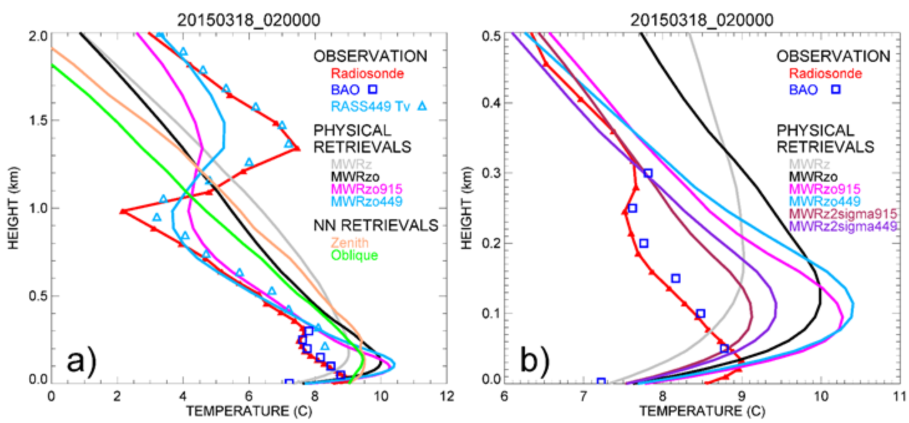

Fig. 5. Panel a~~)~~, as in Fig. 2 but for 18 March 2015 at 0200 UTC. The RASS 449 virtual temperature is included as light blue triangles. Panel b~~)~~ shows the same data ~~(except for the NN retrievals)~~ presented in panel a~~),~~, but only up to 500 m AGL, and includes PR profiles in which the MWR uncertainties were increased by a factor of two, MWRz915 in maroon and MWRz449 in violet.

After several trials, we found that when RASS measurements are included, temperature profiles in this and similar cases exhibiting inversions could be improved -by increasing the random uncertainty of MWR observations, and only using the zenith MWR measurements, because the oblique MWR brightness temperature measurements (which give more information in the lower layer of the atmosphere) seemingly have a bias that competes with the active and more accurate measurements from the RASS and surface observations. In this way, the PR approach is granted more freedom to get an optimal profile in the gap between the

__Formatted:__ Space After: 12 pt, Line spacing: Double, Border: Top: (No border), Bottom: (No border), Left: (No border), Right: (No border), Between : (No border)

lowest RASS measurements and the surface measurement. Proof of this is presented in Figure 5b, that shows the same data as in 5a, but including the profiles obtained when increasing the assumed MWR Tb uncertainties by a factor of two, hereafter called MWRz2sigma915 and MWRz2sigma449, in maroon and violet respectively. The increased accuracy of these temperature profiles compared to MWRzo915 and MWRzo449 are obvious in the layer of atmosphere closer to the surface. Later we will show that these last two PR configurations demonstrate improved statistics over all 58 cases, and also through the layer of the atmosphere up to ~~5km~~5 km. We note that these last two PR configurations, that were found to work well for this dataset, might not be optimal for other datasets. During XPIA the RASS measurements impact (particularly those from the RASS 449) was important in the PR approach. This might not be the case for other datasets or over different seasons, when RASS coverage might not be as good as ~~that~~ during XPIA. For this reason, we think that attention has to be used to determine what is the best configuration to use when dealing with PR approaches. On the positive side, the advantage is that the user can determine and has control on what is the optimal configuration to use in his/her dataset, in terms of different inputs to employ and their relative uncertainty.

4.2 Statistical analysis of ~~PRs compared to NN~~physical retrievals up to 5km AGL

~~Since the iteratively~~ We calculated ~~PRs and the NN retrievals are obtained by very different approaches, we find it very important to compare their~~ the relative statistical behavior~~. We do this~~ of PRs for both ~~for~~ temperature and mixing ratio, providing ~~this~~the comparison in two ways: first ~~using~~to the ~~**Akernel**~~ smoothed radiosonde ~~data obtained~~ using

__Formatted:__ Space After: 12 pt, Line spacing: Double, Border: Top: (No border), Bottom: (No border), Left: (No border), Right: (No border), Between : (No border)

the averaging kernel matrix (as described in section 3.3~~,~~), and second comparing to the original, unsmoothed, radiosonde profiles, just interpolated to the 55 PR vertical levels.

Figure 6 shows the statistical results of these comparisons for temperature, in terms of Pearson correlation, RMSE, and mean bias, averaged over all radiosonde events.

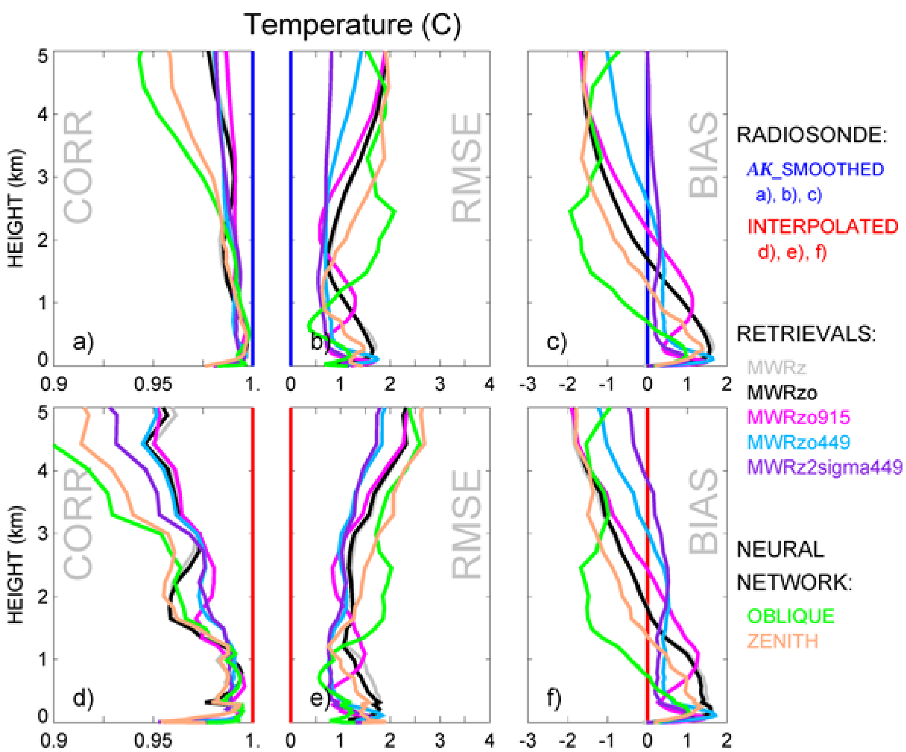

Formatted: *Space After: 12 pt, Line spacing: Double, Border: Top: (No border), Bottom: (No border), Left: (No border), Right: (No border), Between : (No border)*

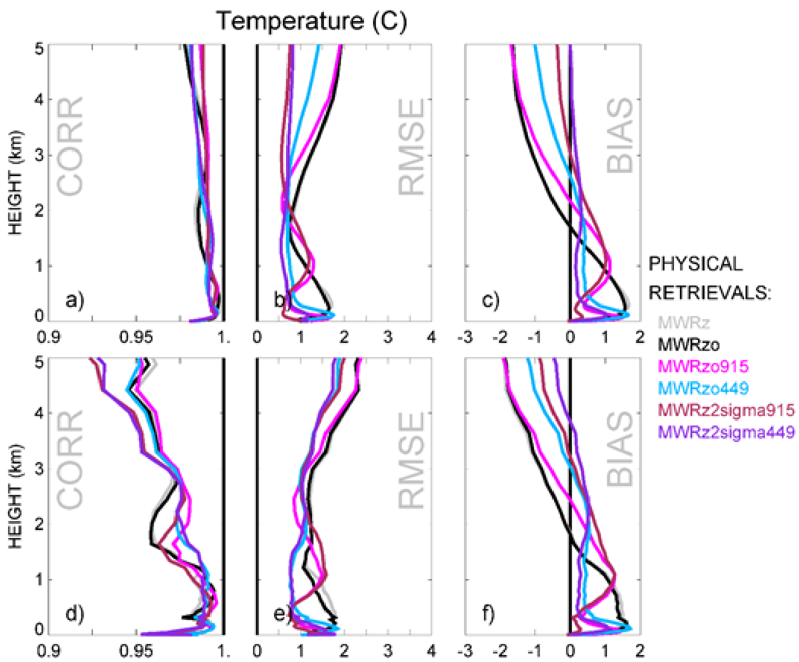

*Fig. 6. Pearson correlation, RMSE, and mean bias for temperature profiles of MWRz in gray, MWRzo in black, MWRzo915 in magenta, MWRzo449 in light-blue, MWRz2sigma915 in maroon and MWRz2sigma449 in violet, computed comparing to smoothed radiosonde data (using their relative **ATkernel**) in panels a-c, and against the original radiosonde measurements in panels d-f. ~~The same comparisons for NN profiles, with NN zenith in beige, and NN averaged oblique in green, are made against the corresponded smoothed radiosonde data in the top panel and against original radiosonde data in the bottom panel.~~*

Formatted: *Space After: 12 pt, Line spacing: Double, Border: Top: (No border), Bottom: (No border), Left: (No border), Right: (No border), Between : (No border)*

These results confirm the superiority of the MWRz2sigma449 temperature retrieval over the other PRs. While this is not true at all heights, this retrieval shows improved distribution of RMSE and bias for the atmospheric layer up to 5 km AGL. The differences between the MWRz2sigma915 ~~profile is not included in the figure to not overcrowd it, but its behaviour compared to~~and the MWRzo915 ~~is~~profiles are similar to ~~that of~~those between the MWRz2sigma449 ~~compared to~~and the MWRzo449 ~~profile~~profiles, reducing the drastic bias found in the layer closer to the ground. The differences between the two ways of comparison, against the smoothed **ATkernel** or the original radiosonde data, are small in terms of RMSE and bias, but more evident in terms of correlation as ~~it~~ can be expected because of the smoothing technique applied to the radiosonde profiles through Eq. (3). Above and below ~1.~~5~~6 km AGL the bias, RMSE, and correlation profiles of the PRs show very different behavior. While statistical ~~measures~~scores above ~1.~~5~~6 km AGL are very similar for the four PRs introduced in Table 1, they are better for the MWRz2sigma915 and MWRz2sigma449 ~~PR~~PRs, especially when compared to the smoothed radiosonde profiles. Differences between the profiles show more variability in the lowest ~~1.5 km. NN retrievals, both for zenith and averaged oblique, are very variable from height to height and generally have much larger RMSE and bias, and worse correlation coefficients compared to PRs.~~~1.6 km where most of the active RASS measurements are available. Also, while both PR profiles related to the RASS 449, MWRzo449 and MWRz2sigma449, have almost constant bias and RMSE from 200m up to at least 3 km, the RASS 915 based PR profiles, MWRzo915 and MWRz2sigma915, have biases and RMSEs that vary with height. Due to the lower first range gate of the RASS 915 measurements, the PR profile of MWRz2sigma915 has the smallest bias and RMSE compared to all other PR profiles in

Formatted: Space After: 12 pt, Line spacing: Double, Border: Top: (No border), Bottom: (No border), Left: (No border), Right: (No border), Between : (No border) the surface to 200 m layer. With quickly decreasing availability of RASS 915 measurement above this layer, the bias and RMSE of MWRzo915 and MWRz2sigma915 became larger, and in some higher layers even larger than the corresponding statistical measures of MWRz and MWRzo. This marks the importance of active measurements spanning a prominent vertical layer to provide a useful application of these data in a radiative transfer model.

Besides temperature profiles, the ~~NN and~~ PR retrievals also provide water vapor mixing ratio profiles.~~-~~ It is understandable that the different configurations of PRs are not noticeably different from each other in relation to moisture, because the Tv observations from the RASS are dominated by the ambient temperature (not moisture), and thus have little impact on the water vapor retrievals.

~~-~~Figure 7 includes the two **AQkernels** corresponding to the PRs MWRz and MWRzo449 in panels a and b, which are averaged over all radiosonde events and appear to be almost identical. More detailed statistical estimations of PRs mixing ratio in Fig 7 c-e, also averaged through all radiosonde events, show very similar correlations, RMSEs, and biases for all PRs included in the figure, meaning that the impact of including RASS observations is minimal on this variable. ~~These PR mixing ratio profiles are also statistically very close to the averaged oblique NN retrieval mixing ratio profiles, with the zenith NN retrieval mixing ratio profiles showing the worst statistics in terms of RMSE and bias. Overall, we conclude that the PR retrievals are not degraded on average compared to the NN moisture retrievals.~~

Formatted: *Space After: 12 pt, Line spacing: Double, Border: Top: (No border), Bottom: (No border), Left: (No border), Right: (No border), Between : (No border)*

Formatted: *Space After: 12 pt, Line spacing: Double, Border: Top: (No border), Bottom: (No border), Left: (No border), Right: (No border), Between : (No border)*

700

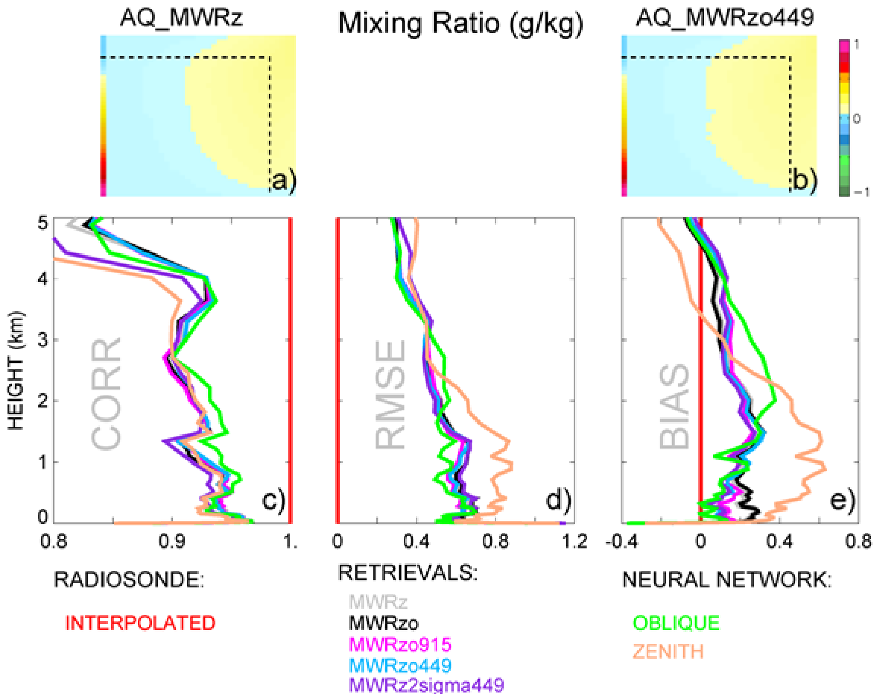

Formatted: Space After: 12 pt, Line spacing: Double, Border: Top: (No border), Bottom: (No border), Left: (No border), Right: (No border), Between : (No border)

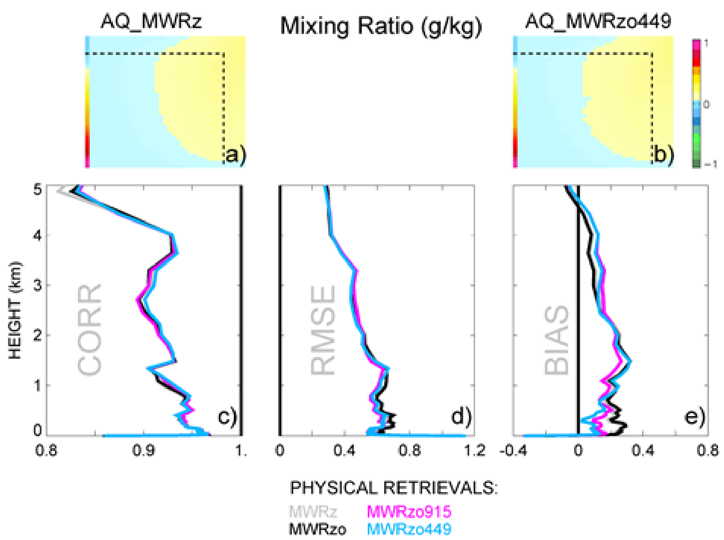

Fig. 7. Top two-color images: ***AQkernels*** *for MWRz (panel a) and MWRzo449 (panel b), averaged over all radiosonde events and shown up to 3 km AGL with dash lines mark 2 km AGL on both panels. Bottom three panels are the same as panels d-f in Figure 6, but for mixing ratio estimation.*

4.3 Statistics for cases far from the climatological mean

~~While both approaches, physical and neural network retrievals, are quite different, both~~Physical retrievals use climatological data as a constraint or for building the statistical relationships used in the retrieval. Statistically, the averaged profiles of both temperature and moisture variables are very close to the climatological averages. However, the most interesting

Formatted: *Space After: 12 pt, Line spacing: Double, Border: Top: (No border), Bottom: (No border), Left: (No border), Right: (No border), Between : (No border)*

and difficult profiles to retrieve are the cases furthest from the climatology (Löhnert and Maier, 2012). To check the behavior of the retrieved data in such events, we first calculated the RMSE for each radiosonde profile relative to the prior profiles for 42 vertical levels from the surface up to 5 km AGL, and then we selected the 15 cases with the largest 0-5km layer averaged RMSEs compared to the prior. All comparisons are done against the corresponded smoothed **ATkernel** radiosonde data, using **AT_MWRz, AT_MWRzo, AT_MWRzo915, AT_MWRzo449, AT_MWRz2sigma915, AT_MWRz2sigma449** for all six PRs~~, and **AT_MWRz, AT_MWRzo** for NN zenith and NN oblique retrievals respectively~~.

Formatted: *Space After: 12 pt, Line spacing: Double, Border: Top: (No border), Bottom: (No border), Left: (No border), Right: (No border), Between : (No border)*

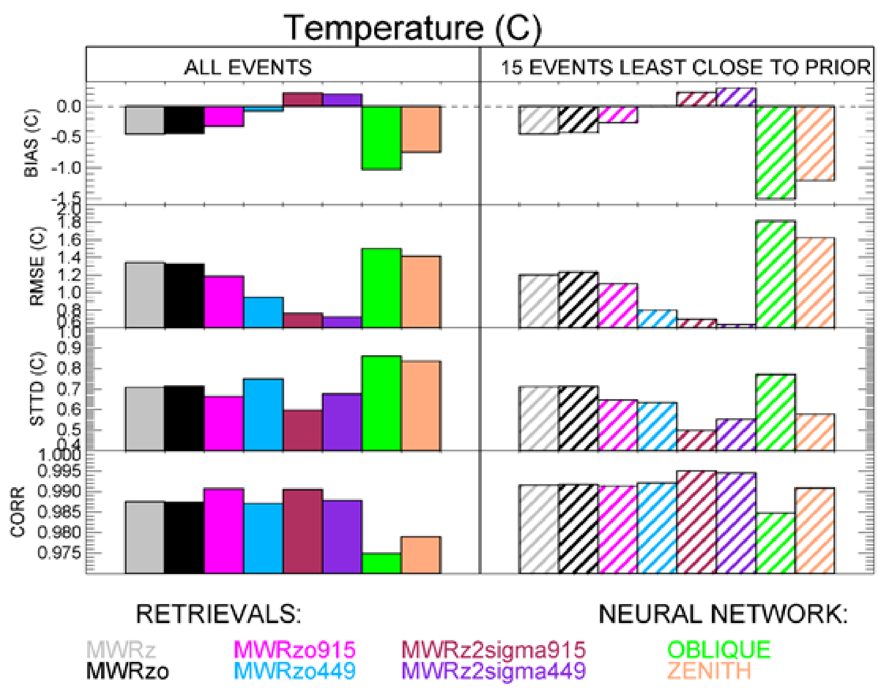

Formatted: Space After: 12 pt, Line spacing: Double, Border: Top: (No border), Bottom: (No border), Left: (No border), Right: (No border), Between : (No border)

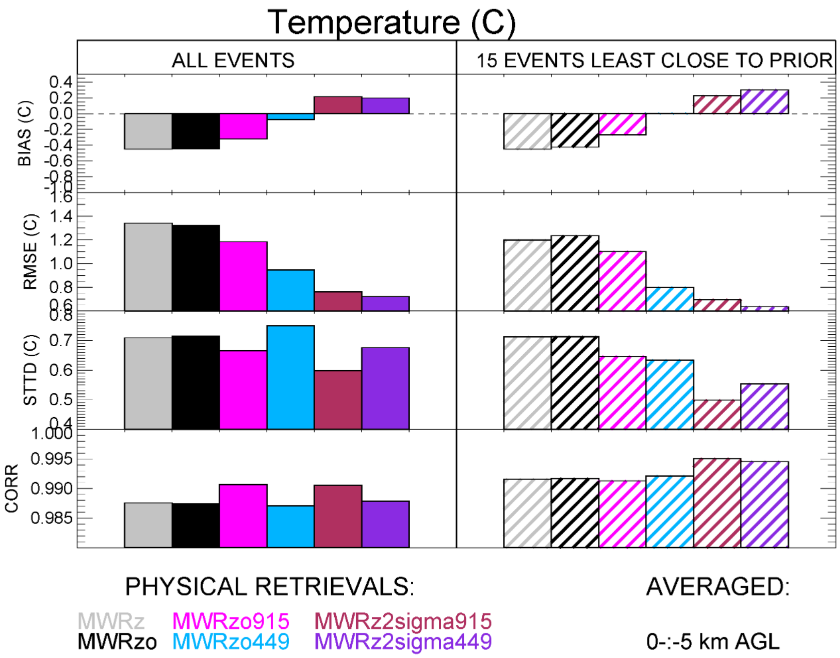

Fig. 8. From top to bottom: biases (retrievals minus ATkernel radiosonde), RMSEs, standard deviations of the difference between retrievals and ATkernel radiosonde, and Pearson correlations for the six PR configurations so far introduced~~ and both NN retrievals~~, averaged from the surface to 5 km AGL, averaged over all radiosonde data (solid boxes), and averaged over the 15 events furthest from the priors (hatched boxes).

Figure 8 shows the temperature statistical analysis for the entire radiosonde data set (solid boxes) and to just the fifteen chosen events (hatched boxes) for bias, RMSE, standard deviation of retrieval differences to the radiosonde data, and Pearson correlation, calculated as

Formatted: *Space After: 12 pt, Line spacing: Double, Border: Top: (No border), Bottom: (No border), Left: (No border), Right: (No border), Between : (No border)*

the weighted averaged over the 42 vertical heights up to 5 km AGL. The vertical resolution of the Physical Retrievals is not uniform, with more frequent levels closer to the surface. If a simple average of the data from all levels is used, the near-surface layer will be weighted more compared to the upper levels of the retrievals. To avoid this, a vertical average over the lowest 5km AGL is performed using weights at each vertical level determined by the distance between the levels. Differences in the statistics when using the entire radiosonde data set or the fifteen profiles furthest from the prior are noticeable, especially for bias and RMSE, but also for the standard deviation. All PRs that include RASS observations show better performance compared to strictly MWR-only PR profiles (i.e., MWRz and MWRzo) for almost all statistical comparisons. Also, the statistical behavior of the MWRz2sigma915 and MWRz2sigma449 retrievals are the best in terms of RMSE and standard deviation for all events and for RMSE, standard deviation, and correlation coefficient, for the fifteen profiles furthest from the climatological average. Fig. ~~Finally, we note~~8 also shows that ~~the NN profiles are the least accurate retrievals for all of the statistics for the entire radiosonde data set,~~RMSE, standard deviation and ~~have the highest bias, RMSE and the lowest~~ correlation have improved scores for the 15 events furthest from the prior when compared to all temperature profiles for all PRs using active RASS measurements.

__Formatted:__ Space After: 12 pt, Line spacing: Double, Border: Top: (No border), Bottom: (No border), Left: (No border), Right: (No border), Between : (No border)

749

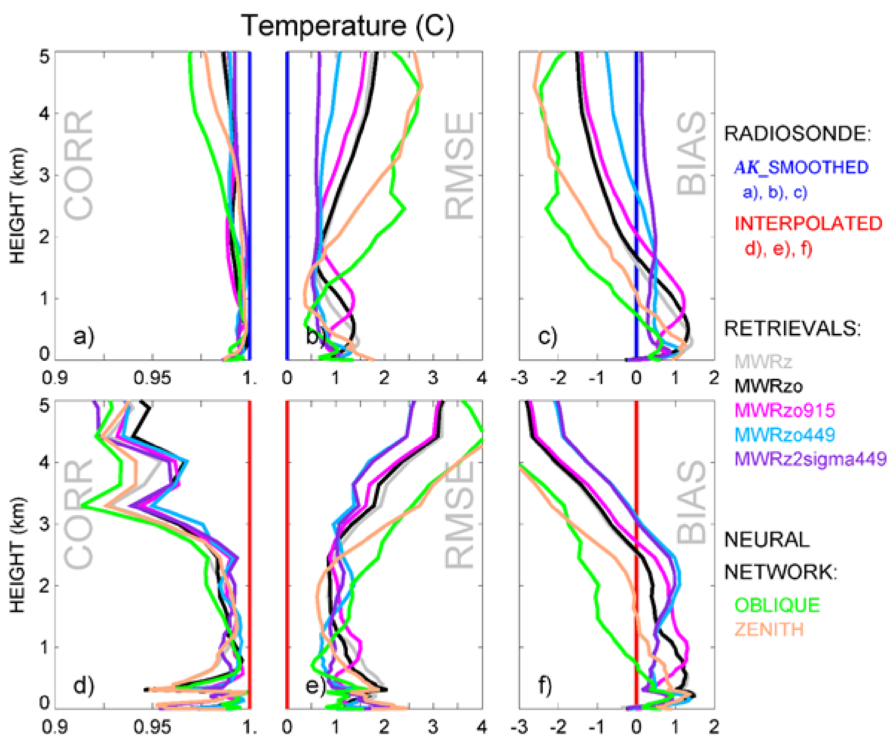

Formatted: Space After: 12 pt, Line spacing: Double, Border: Top: (No border), Bottom: (No border), Left: (No border), Right: (No border), Between : (No border)

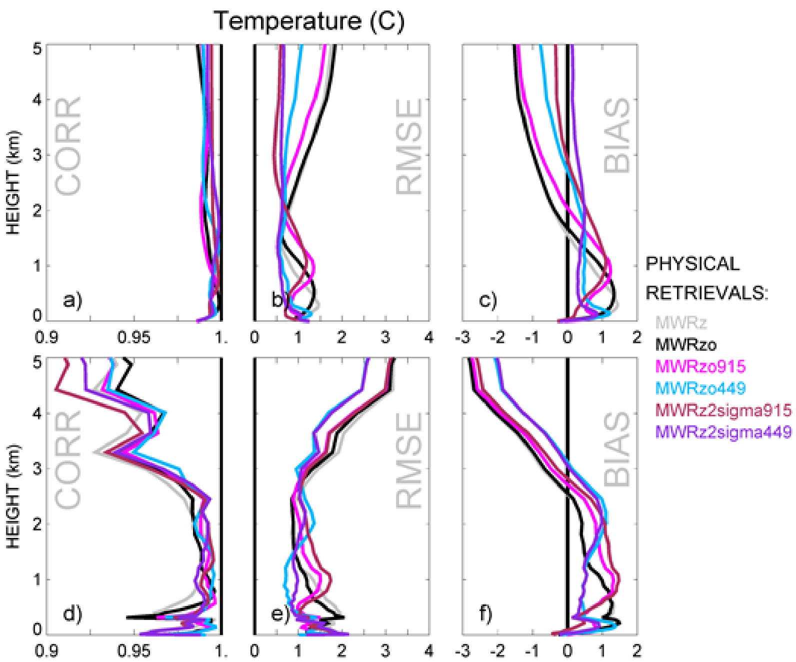

Fig. 9. The same as Fig. 6 but for the temperature over 15 furthest from prior radiosonde profiles.

To investigate the vertical structure of the error statistics for the 15 events furthest from the radiosonde climatology, profiles of correlation, RMSE and bias for these events are shown in Figure 9 for the layer 0-5 km. ~~-~~The ~~MWRz449~~MWRz2sigma915 and MWRz2sigma449 profiles, ~~which were seen in~~ having~~Fig. 8 to have~~ the best ~~layer~~ averaged statistics in Fig. 8, are seen ~~to be~~ as good as, or better, than the other methods for the 0-2 km layer.~~-~~ Importantly, for heights above 2km AGL, where there is no additional observational data from RASS, all of the PRs ~~are~~

Formatted: *Space After: 12 pt, Line spacing: Double, Border: Top: (No border), Bottom: (No border), Left: (No border), Right: (No border), Between : (No border)*

~~better than the NN profiles, with the MWRz2sigma449 and MWRz449 being the best. We note that the increased accuracy of the PRs relative to the NNs is more obvious in Fig. 9 for the 15 events when compared to the entire data set in~~ with RASS are closer to the “true” radiosonde temperature compared to the PRs without RASS.~~Fig. 6. Also, it can be seen that the NNs for the 15 events are worse than they are for the entire data set, especially in the 2-5km layer, which indicates (not surprisingly) that the NNs accuracy degrades when the atmosphere is far from its climatology.~~

4.4 Virtual temperature statistics

The above analysis confirms the superiority of MWRz2sigma915 and MWRz2sigma449 compared to the other PRs ~~and to the NN retrievals~~ for this dataset. In this section we show the direct comparison of the retrieved profiles to the original radiosonde and RASS virtual temperature profiles. Using temperature and moisture retrieval output, we calculated “retrieved virtual temperature profiles” and interpolated all profiles and RASS data on a regular vertical grid, going from 200 m to 1.6 km with 100 m range, for easy comparison.

Figure 10 shows Tv retrieved profile biases compared to the original radiosonde data as solid lines, and RASS 915 and RASS 449 Tv bias as asterisks. A zero bias is denoted by the red line. On the left side of the figure we show bar charts of the RASS measurement availability as a function of height. The widest part of these charts corresponds to 100% data availability. Heights with RASS availability greater than 50% are marked with additional circles over the asterisks.

Formatted: *Space After: 12 pt, Line spacing: Double, Border: Top: (No border), Bottom: (No border), Left: (No border), Right: (No border), Between : (No border)*

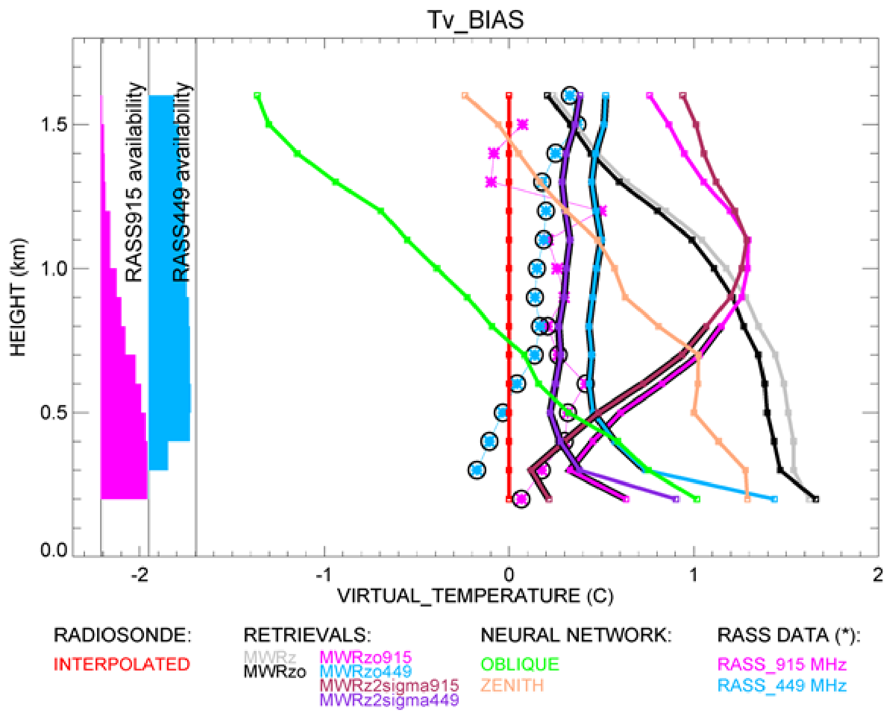

Formatted: *Space After: 12 pt, Line spacing: Double, Border: Top: (No border), Bottom: (No border), Left: (No border), Right: (No border), Between : (No border)*

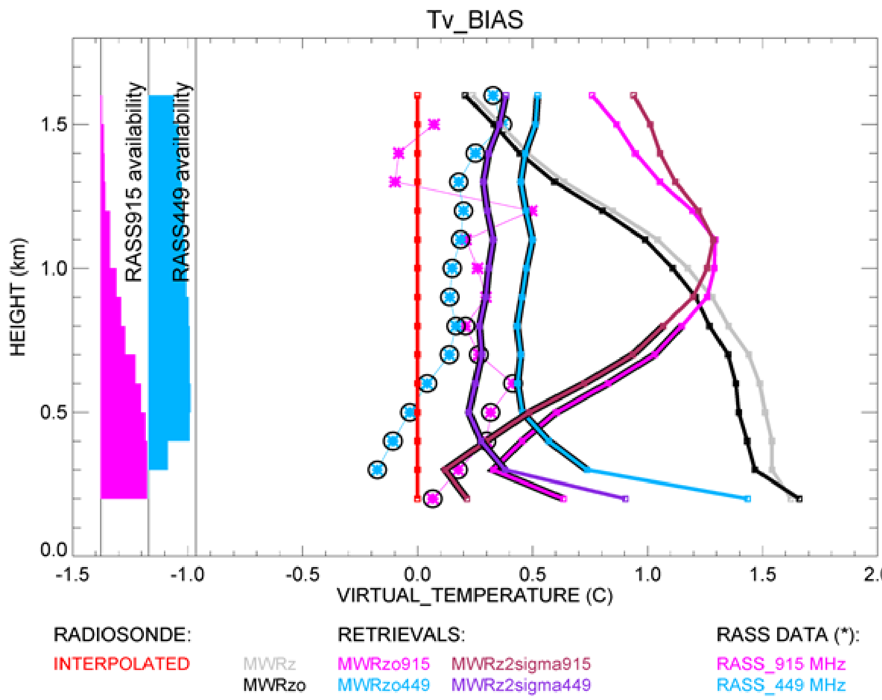

Fig. 10. Bias of virtual temperature for all six PR configurations ~~and both NN retrievals~~ compared to the original radiosonde measurements. RASS data are marked by asterisks and by additional circles for the RASS data with more than 50% availability, according to the availability bar charts on the left.

While RASS 449 data are available at almost all heights up to 1.6 km, the RASS 915 data availability decreases considerably with height, lowering to 50% availability around 800 m AGL. All PRs with input from RASS data, MWRzo915 and MWRzo449, and MWRz2sigma915 and MWRz2sigma449~~ with larger MWR uncertainties~~, are also marked with additional black lines at

Formatted: *Space After: 12 pt, Line spacing: Double, Border: Top: (No border), Bottom: (No border), Left: (No border), Right: (No border), Between : (No border)*

the heights with at least 50% of relative RASS data availability. This figure clearly shows the superiority of MWRz2sigma449 and MWRz2sigma915 (in the layer with > 50% RASS 915 data availability) compared to MWRz and MWRzo configurations, which do not include RASS data, as well as to MWRzo915 and MWRzo449 which include RASS data and MWR zenith and oblique data. For MWRzo449 and MWRz2sigma449 profiles, RASS 449 data were almost always available, therefore it is easy to identify similar features between Tv bias profiles of the RASS 449 and the PRs including it. Thus, for the MWRzo449 and MWRz2sigma449 the Tv bias is more uniform through the heights compared to all other PRs that do not include RASS data~~, and to both NN retrievals.~~. Moreover, because MWRzo449 and MWRz2sigma449 Tv bias profiles follow tightly the trend of the RASS 449 with height, the difference between MWRzo449 and RASS 449 biases equals ~0.32 °C and the difference between MWRz2sigma449 and RASS 449 biases equals ~0.14 °C over the ~1.3 km atmospheric layer where most of RASS 449 measurements are available, uniformly distributed through the heights. Finally, the average differences between these MWRzo449 and MWRz2sigma449 Tv profiles and the radiosonde virtual temperature equal ~0.56 °C and ~0.34 °C respectively. ~~From these results we can assume that the final bias of the PRs that include additional RASS data derives from a combination of the RASS data bias itself, of the uncertainty of the retrieval model, and of the MWR brightness temperature biases, even though we tried to correct for the latter.~~

We note that as an alternative to using the PR ~~temperatures~~temperature profiles at all heights, one could consider replacing the PR temperatures with RASS observations up to the maximum height reached by the RASS, and then use the PR retrieval above that. ~~-~~To do this the

Formatted: *Space After: 12 pt, Line spacing: Double, Border: Top: (No border), Bottom: (No border), Left: (No border), Right: (No border), Between : (No border)*

moisture contribution to the RASS virtual temperatures could be removed by using either the relative humidity measured by radiometer or by a climatology of the moisture term.

5. Conclusions

In this study we used the data collected during the XPIA field campaign to test different configurations of a physical-iterative retrieval (PR) approach in the determination of temperature and humidity profiles from data collected by microwave radiometers, surface sensors, and RASS measurements. We tested the accuracy of several PR configurations, two that made use only of surface observations and MWR observed brightness temperature (zenith only, MWRz, and zenith plus oblique, MWRzo), and others that included the active observations available from two co-located RASS (one, RASS 915, associated with a 915-MHz, and the other, RASS 449, associated with a 449-MHz wind profiling radar). Radiosonde launches were used for verification of the retrieved profiles and Neural Network retrieved profiles were also used for comparison~~. The NN retrievals used in this study were obtained either using the zenith angle only, or the average of the oblique scans (based on the averaged Tb of 15- and 165-degree scans) without including the zenith. Other MWR systems (Rose et al., 2005) provide retrieved profiles that include the information from both oblique and zenith scans.~~ (see Appendix A).

Formatted: *Outline numbered + Level: 1 + Numbering Style: 1, 2, 3, … + Start at: 1 + Alignment: Left + Aligned at: 0.25" + Indent at: 0.5"*

Formatted: *Space After: 12 pt, Line spacing: Double, Border: Top: (No border), Bottom: (No border), Left: (No border), Right: (No border), Between : (No border)*

Inclusion of the observations from the active RASS instruments in the PR approach improves the accuracy of the temperature profiles, particularly when ~~low-level~~ temperature inversions are present. Of the PRs configurations tested, we find better statistical agreement with the radiosonde observations when the RASS 449 is used together with the surface observations and brightness temperature from only the zenith MWR observations ~~(MWRz2sigma449),~~ and doubling the random radiometric uncertainty on the MWR observations (MWRz2sigma449) relative to the uncertainty calculated over the selected clear-sky days ~~(Fig. 1).~~. This configuration is also more accurate compared to MWRzo915 or MWRz2sigma915 (which use RASS 915 observation), because of the deeper RASS 449 height coverage. ~~-~~The larger assumed radiometric uncertainty in the MWR Tb observations allows the retrieval to overcome both (a) the ~~(~~small~~)~~ systematic errors that exist between the MWR ~~(which could be in either the~~ observed Tb values ~~or in the MonoRTM used as the forward model)~~ and the RASS~~,~~ measurements and (b) the systematic errors that exist in forward microwave radiative models (Cimini et al. 2018).

We also selected 15 cases when temperature profiles from the radiosonde observations were the furthest from the mean climatological average, and reproduced the statistical comparison over this subset of cases. These are the cases usually the most difficult to retrieve and the most important to forecast; therefore, it is essential to improve the retrievals in these

Formatted: *Space After: 12 pt, Line spacing: Double, Border: Top: (No border), Bottom: (No border), Left: (No border), Right: (No border), Between : (No border)*

situations. Even for this subset of selected cases we find that MWRz2sigma449 produces better statistics, proving that the inclusion of active sensor observations in MWR passive observations would be beneficial for improving the accuracy of the retrieved temperature profiles also in the upper layer of the atmosphere where RASS measurements are not available (at least up to 5 km AGL). However, we note that this result may be dependent on the fact that our oblique measurements were taken at a 15-degree elevation angle, and that MWRs in locations with unobstructed views allowing for scans down to 5 degrees may provide similar improvements to the temperature profile accuracy in the lowest 0-1 or even 0-2 km AGL layers (Crewell and Löhnert, 2007).

Finally, we also considered the impact of the inclusion of RASS measurements on the retrieved humidity profiles, but in this case the inclusion of RASS observations did not produce significantly better results, compared to the configurations that do not include them. This was not a surprise as RASS measures virtual temperature, effectively adding very little extra information to the water vapor retrievals. In this case a better option would be to consider adding other active remote sensors such as water vapor differential absorption lidars (DIALs) to the PRs. Turner and Löhnert (2020) showed that including the partial profile of water vapor observed by the DIAL substantially increases the information content in the combined water

Formatted: *Space After: 12 pt, Line spacing: Double, Border: Top: (No border), Bottom: (No border), Left: (No border), Right: (No border), Between : (No border)*

vapor retrievals. Consequently, to improve both temperature and humidity retrievals a synergy between MWR, RASS, and DIAL systems would likely be necessary.

Appendix A

The XPIA NN retrievals use a training dataset based on a 5-year climatology of profiles from radiosondes launched at the Denver International Airport, 35 miles south-east from the XPIA site. NN-based MWR vertical retrieval profiles were obtained using the zenith or an average of two oblique elevation scans, 15- and 165-degrees, all with 58 levels extending from the surface up to 10 km, with nominal vertical levels depending on the height (every 50 m from the surface to 500 m, every 100 m from 500 m to 2 km, and every 250 m from 2 to 10 km, AGL).

Fig. 1A shows composite NN vertical profiles of temperature (separately for the zenith and averaged obliques) calculated for radiosonde launch times, and the corresponding PR profiles already introduced in Fig. 6. As expected, the averaged oblique NN profile has lower bias and RMSE compared to the zenith NN profile below 1km AGL, while the zenith NN profile improved above this level.

Formatted: *Space After: 12 pt, Line spacing: Double, Border: Top: (No border), Bottom: (No border), Left: (No border), Right: (No border), Between : (No border)*

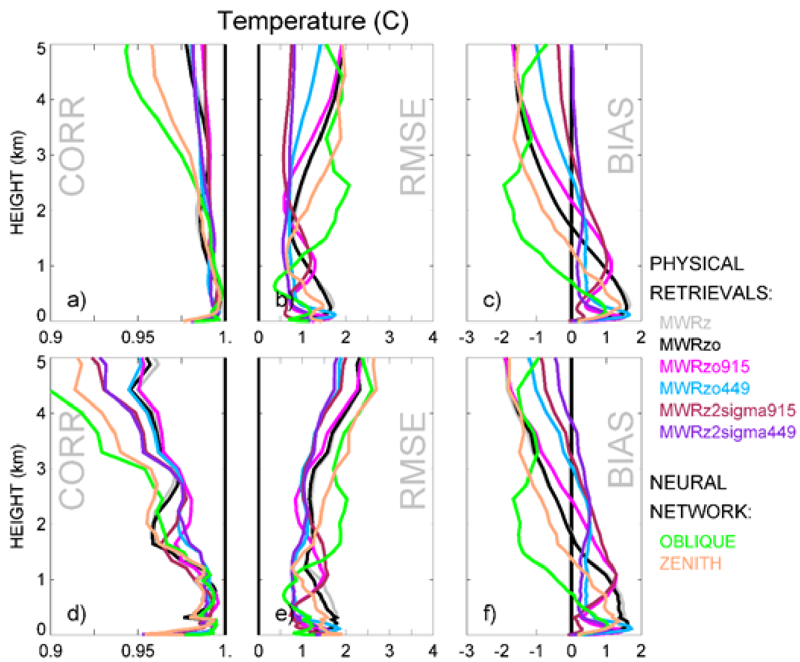

Fig. 1A. The same as Fig. 6 but with additional NN temperature profiles, from zenith in beige and from averaged oblique – in green.

We note that in this comparison the MWR Tb data have been bias-corrected before being used in the Physical Retrieval configurations, as discussed in Section 3.2, while the NN retrievals use the uncorrected Tb, since it was non-trivial for us to reprocess those retrievals. Zenith NN profiles have larger bias and RMSE and smaller correlation coefficient above 1 km

Formatted: *Space After: 12 pt, Line spacing: Double, Border: Top: (No border), Bottom: (No border), Left: (No border), Right: (No border), Between : (No border)*

AGL compared to all PR profiles. This is possibly due to the Tb bias in the transparent channels of the V-band frequencies.

To optimize the use of the two types of NN scan data, we combined the NN retrieved profiles using only the averaged oblique scans up to 1 km AGL and the zenith scans above 1 km. Fig. 2A is the same as Fig. 8, now including also the three NN profiles (averaged oblique only, zenith only, and their combination) presenting the statistics in three different layers of atmosphere: from the surface to 5 km AGL, from the surface to 2 km AGL, and from the surface to 1 km AGL (a, b and c panels).

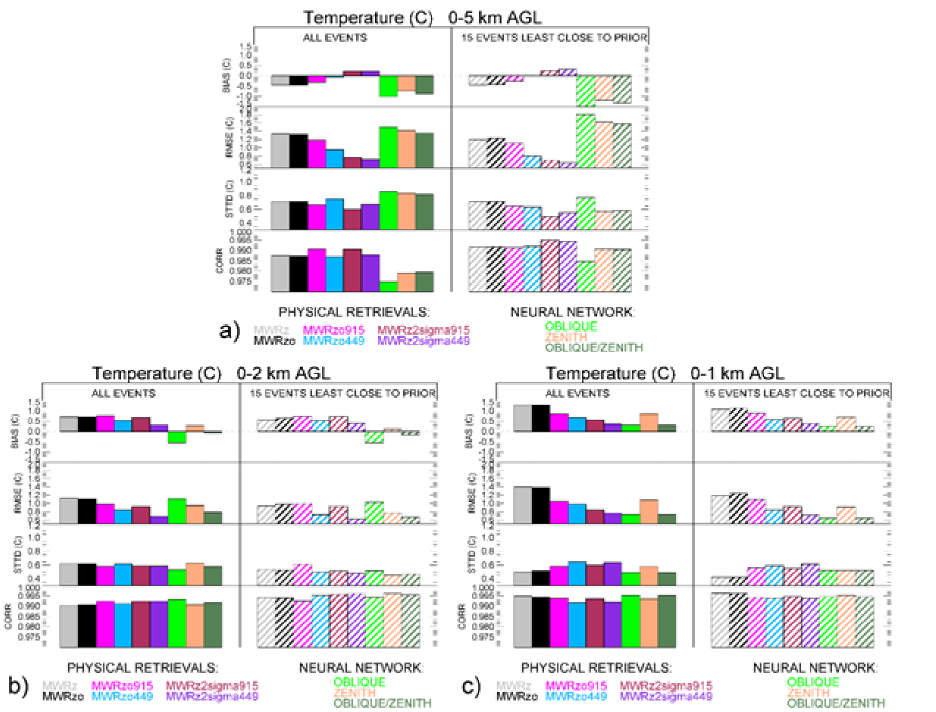

Formatted: Space After: 12 pt, Line spacing: Double, Border: Top: (No border), Bottom: (No border), Left: (No border), Right: (No border), Between : (No border)

Fig. 2A. The same as Fig. 8 but including NN profile statistics from averaged oblique scans in beige, from zenith – in green, and from their combination – in spruce. Panels a, b, and c show the temperature statistics from the surface up to 5, 2 and 1 km AGL respectively.

Oblique only (and oblique and zenith combined) NN profiles show the best statistics in the layer closest to the surface, up to 1 km AGL, panel c, while in the deeper atmosphere layer up to 5 km all PR profiles have improved statistics compared to NNs, panel a. Panel b has mixed results: MWRz2sigma449 has the lowest RMSE, and the combined NN retrieved profiles show just slightly larger RMSE and almost the same standard deviation and correlation. It is important to admit that while potential NN bias-correction generally cannot change the oblique statistics, it may improve the zenith profiles, especially above 1 km AGL, therefore improving the combined NN profiles statistics.

Data availability

All data are publicly accessible at the DOE Atmosphere to Electrons Data Archive and Portal, found at https://a2e.energy.gov/projects/xpia (Lundquist et al., 2016).

Author contribution

Irina Djalalova completed the primary analysis with physical retrieval approach through MONORTM using XPIA data. Daniel Gottas contributed to the post-processing of the RASS data. Irina Djalalova prepared the manuscript with contributions from all co-authors.

__Formatted:__ Space After: 12 pt, Line spacing: Double, Border: Top: (No border), Bottom: (No border), Left: (No border), Right: (No border), Between : (No border)

Acknowledgements

We thank all the people involved in XPIA for instrument deployment and maintenance, data collection, and data quality control, and particularly the University of Colorado Boulder for making the CU MWR data available. Funding for this study was provided by the NOAA/ESRL Atmospheric Science for Renewable Energy (ASRE) program.

Formatted: *Indent: First line: 0"*

References

Adachi, A. and H. Hashiguchi, 2019: Application of parametric speakers to radio acoustic sounding system. *Atmos. Meas. Tech.*, **12**, 5699–5715, 2019, https://doi.org/10.5194/amt-12-5699-2019.

Adler, B., J. M. Wilczak, L. Bianco, I. Djalalova, J. B. Duncan Jr., D. D. Turner, ~~2020~~2021: Observational case study of a persistent cold air pool and gap flow in the Columbia River Basin. *Under review to J. of Appl.* ~~*In preparation*~~*Meteor. Climatol*.

Banta, R. M., and coauthors, 2020: Characterizing NWP model errors using Doppler lidar measurements of recurrent regional diurnal flows: Marine-air intrusions into the Columbia River Basin. *Month. Wea. Rev.*, **148**, 927-953, ~~doi:10.1175/MWR-D-19-0188.1~~https://doi.org/10.1175/MWR-D-19-0188.1

Formatted: *Border: Top: (No border), Bottom: (No border), Left: (No border), Right: (No border), Between : (No border)*

Formatted: *Space After: 12 pt, Line spacing: Double, Border: Top: (No border), Bottom: (No border), Left: (No border), Right: (No border), Between : (No border)*

~~Blumberg, W. G., D. D. Turner, S. M. Cavallo, J. Gao, J. Basara, A. Shapiro, 2019: An Analysis of the Processes Affecting Rapid Near-Surface Water Vapor Increases during the Afternoon to Evening Transition in Oklahoma. J. of Appl. Meteorol. and Climatol., 58(10), 2217–2234, https://doi.org/10.1175/JAMC-D-19-0062.1.~~

Bianco L., D. Cimini, F. S. Marzano, and R. Ware, 2005: Combining microwave radiometer and wind profiler radar measurements for high-resolution atmospheric humidity profiling, *J. Atmos. Ocean. Tech.*, **22**, 949–965, https://doi.org/10.1175/JTECH1771.1.

Bianco, L., K. Friedrich, J. M. Wilczak, D. Hazen, D. Wolfe, R. Delgado, S. Oncley, and J. K. Lundquist, 2017: Assessing the accuracy of microwave radiometers and radio acoustic sounding systems for wind energy applications. *Atmos. Meas. Tech.*, **10**, 1707-1721, https://doi.org/10.5194/amt-10-1707-2017.

Cadeddu, M. P., J. C. Liljegren, and D. D. Turner, 2013: The Atmospheric radiation measurement (ARM) program network of microwave radiometers: instrumentation, data, and retrievals, *Atmos. Meas. Tech.*, **6**, 2359–2372, https://doi.org/10.5194/amt-6-2359-2013.

Cimini, D., T. J. Hewison, L. Martin, J. Guldner, C. Gaffard, F. S. Marzano, 2006: Temperature and humidity profile retrievals from ground-based microwave radiometers during TUC, Meteorologische Zeitschrift, Vol. 15, No. 5, 45-56, DOI: 10.1127/09411-D-2948/2006/0099

Cimini, D., E. Campos, R. Ware, S. Albers, G. Giuliani, J. Oreamuno, P. Joe, S. E. Koch, S. Cober, and E. Westwater, 2011: Thermodynamic Atmospheric Profiling during the 2010 Winter

Formatted: *Space After: 12 pt, Line spacing: Double, Border: Top: (No border), Bottom: (No border), Left: (No border), Right: (No border), Between : (No border)*

Olympics Using Ground-based Microwave Radiometry, *IEEE Trans. Geosci. Remote Sens.*, **49**, 12, https://doi.org/10.1109/TGRS.2011.2154337.

Cimini, D., Rosenkranz, P. W., Tretyakov, M. Y., Koshelev, M. A., and Romano, F., 2018: Uncertainty of atmospheric microwave absorption model: impact on ground-based radiometer simulations and retrievals, *Atmos. Chem. Phys.*, **18**, 15231–15259, https://acp.copernicus.org/articles/18/15231/2018/.

Cimini, D., M. Haeffelin, S. Kotthaus, U. Löhnert, P. Martinet, E. O'Connor, C. Walden, M. Collaud Coen, and J. Preissler, 2020: Towards the profiling of the atmospheric boundary layer at European scale—introducing the COST Action PROBE. *Bulletin of Atmospheric Science and Technology*, **1**, 23–42, https://doi.org/10.1007/s42865-020-00003-8.

~~Cimini, D., Rosenkranz, P. W., Tretyakov, M. Y., Koshelev, M. A., and Romano, F., 2018: Uncertainty of atmospheric microwave absorption model: impact on ground-based radiometer simulations and retrievals, *Atmos. Chem. Phys.*, **18**, 15231–15259, https://acp.copernicus.org/articles/18/15231/2018/.~~

Clough, S.A., M. W. Shephard, E. J. Mlawer, J. S. Delamere, M. Iacono, K. E. Cady-Pereira, S. Boukabara and P. D. Brown, 2005: Atmospheric radiative transfer modeling: A summary of the AER codes, *JQSRT*, vol 91, no. 2, pp 233-244, ~~2005,~~ https://doi.org/10.1016/j.jqsrt.2004.05.058.

Crewell, S., U. Löhnert, 2007: Accuracy of Boundary Layer Temperature Profiles Retrieved With Multifrequency Multiangle Microwave Radiometry, IEEE TGRS, VOL. 45, NO. 7, JULY 2007, DOI: 10.1109/TGRS.2006.888434.

Formatted: *Font color: Custom Color(RGB(17,85,204))*

Formatted: *Space After: 12 pt, Line spacing: Double, Border: Top: (No border), Bottom: (No border), Left: (No border), Right: (No border), Between : (No border)*

Engelbart, D., W. Monna, J. Nash, 2009: Integrated Ground-Based Remote-Sensing Stations for Atmospheric Profiling, *COST Action 720 Final Report*, EUR 24172, https://doi.org/10.2831/10752.

Görsdorf, U., and V. Lehmann, 2000: Enhanced Accuracy of RASS-Measured Temperatures Due to an Improved Range Correction. J. Atmos. Oceanic Technol., **17 (4)**, 406–416, https://doi.org/10.1175/1520-0426(2000)017<0406:EAORMT>2.0.CO;2.

Han, Y., and E. R. Westwater, 1995: Remote sensing of tropospheric water vapor and cloud liquid water by integrated ground-based sensors. *J. Atmos. Oceanic Tech.*, **12**, 1050-1059~~.~~, DOI: https://doi.org/10.1175/1520-0426(1995)012<1050:RSOTWV>2.0.CO;2

~~Han, Y.,~~Hewison, T., 2007: 1D-VAR Retrieval of Temperature and ~~E. R. Westwater, 2000: Analysis and improvement of tipping calibration for ground-based microwave radiometers.~~Humidity Profiles From a Ground-Based Microwave Radiometer, *IEEE Trans. Geosci. Remote Sens.*, ~~**38,** 1260–1276,~~ **45(7)**, 2163–2168, https://doi.org/10.1109/TGRS.2007.898091. ~~https://doi.org/10.1109/36.843018.~~

Horst, T. W., S. R. Semmer, and I. Bogoev, 2016: Evaluation of Mechanically-Aspirated Temperature/Relative Humidity Radiation Shields, *18th Symposium on Meteorological Observation and Instrumentation, AMS Annual Meeting*, New Orleans, LA, 10-15 January 2016, https://ams.confex.com/ams/96Annual/webprogram/Paper286839.html.

Kaimal, J. C., and J. E. Gaynor, 1983: The Boulder Atmospheric Observatory. *J. Climate Appl. Meteor.*, **22**, 863–880, https://doi.org/10.1175/1520-0450(1983)022<0863:TBAO>2.0.CO;2.

Formatted: *Space After: 12 pt, Line spacing: Double, Border: Top: (No border), Bottom: (No border), Left: (No border), Right: (No border), Between : (No border)*

Küchler, N., D. D. Turner, U. Löhnert,and S. Crewell, 2016: Calibrating ground-based microwave radiometers: Uncertainty and drifts, *Radio Sci.*, **51**, 311–327,doi:10.1002/2015RS005826.

Löhnert U. and O. Maier, 2012: Operational profiling of temperature using ground-based microwave radiometry at Payerne: prospects and challenges. *Atmos. Meas. Tech.*, **5**, 1121–1134, https://doi.org/10.5194/amt-5-1121-2012.

Lundquist, J. K., J. M. Wilczak, R. Ashton, L. Bianco, W. A. Brewer, A. Choukulkar, A. Clifton, M. Debnath, R. Delgado, K. Friedrich, S. Gunter, A. Hamidi, G. V. Iungo, A. Kaushik, B. Kosović, P. Langan, A. Lass, E. Lavin, J. C.-Y. Lee, K. L. McCaffrey, R. K. Newsom, D. C. Noone, S. P. Oncley, P. T. Quelet, S. P. Sandberg, J. L. Schroeder, W. J. Shaw, L. Sparling, C. St. Martin, A. St. Pe, E. Strobach, K. Tay, B. J. Vanderwende, A. Weickmann, D. Wolfe, and R. Worsnop, 2017: Assessing state-of-the-art capabilities for probing the atmospheric boundary layer: the XPIA field campaign. *Bull. Am. Meteor. Soc.*, **98**, 289–314, https://doi.org/10.1175/BAMS-D-15-00151.1.

Maahn, M., D. D. Turner, U. Löhnert, D. J. Posselt, K. Ebell, G. G. Mace, and J. M. Comstock, 2020: Optimal estimation retrievals and their uncertainties: What every atmospheric scientist should know. *Bull. Amer. Meteor. Soc.*, **101**, E1512-E1523, https://doi~~:~~.org/10.1175/BAMS-D-19-0027.1

~~May P. T., Moran, K. P., and Strauch, R. G., 1989: The Accuracy of RASS Temperature Measurements, *J. Appl. Meteorol.*, **28**, 1329–1335.~~

Formatted: *Space After: 12 pt, Line spacing: Double, Border: Top: (No border), Bottom: (No border), Left: (No border), Right: (No border), Between : (No border)*

Maddy, E. S. and C. D. Barnet, 2008: Vertical Resolution Estimates in Version 5 of AIRS Operational Retrievals. *IEEE TGRS*, VOL. **46**, NO. 8, AUGUST 2008, https://doi.org/10.1109/TGRS.2008.917498

Martinet, P., D. Cimini, F. Burnet, B. Ménétrier, Y. Michel, and V. Unger, 2020: Improvement of numerical weather prediction model analysis during fog conditions through the assimilation of ground-based microwave radiometer observations: a 1D-Var study, *Atmos. Meas. Tech.*, **13**, 6593–6611, https://doi.org/10.5194/amt-13-6593-2020.

May, P. T. and J. M. Wilczak, 1993: Diurnal and Seasonal Variations of Boundary-Layer Structure Observed with a Radar Wind Profiler and RASS. Mon. Wea. Rev., **121**, 673–682, https://doi.org/10.1175/1520-0493(1993)121<0673:DASVOB>2.0.CO;2.

Masiello, G., C. Serio, and P. Antonelli, 2012: Inversion for atmospheric thermodynamical parameters of IASI data in the principal components space. *Quart. J. Roy. Meteor. Soc.*, **138**, 103–117, https://doi.org/10.1002/qj.909.

Merrelli, A. M., and D. D. Turner, 2012: Comparing information content of upwelling far infrared and midinfrared radiance spectra for clear atmosphere profiling. *J. Atmos. Oceanic Technol.*, **29**, 510–526, https://doi.org/10.1175/JTECH-D-11-00113.1.

Neiman, P. J., D. J. Gottas, and A. B. White, 2019: A Two-Cool-Season Wind Profiler–Based Analysis of Westward-Directed Gap Flow through the Columbia River Gorge. *Month. Wea. Rev.*, **147**, 4653-4680, https://doi.org/10.1175/MWR-D-19-0026.1.

North, E. M., A. M.Peterson, and H. D. Parry , 1973: RASS, a remote sensing system for measuring low-level temperature profiles. *Bull. Am. Meteor. Soc.*, **54**, 912–919.

Formatted: *Space After: 12 pt, Line spacing: Double, Border: Top: (No border), Bottom: (No border), Left: (No border), Right: (No border), Between : (No border)*

Payne, V. H., J. S. Delamere, K. E. Cady-Pereira, R. R. Gamache, J.-L. Moncet, E. J. Mlawer, and S. A. Clough, 2008: Air-broadened half-widths of the 22- and 183-GHz water-vapor lines. *IEEE Trans. Geosci. Remote Sens.*, **46**, 3601-3617, ~~doi:10.1109/TGRS.2008.2002435.~~https://doi.org/10.1109/TGRS.2008.2002435.

Payne, V. H., E. J. Mlawer, K. E. Cady-Pereira, and J.-L. Moncet, 2011: Water vapor continuum absorption in the microwave. *IEEE Trans. Geosci. Remote Sens.*, **49**, 2194-2208, ~~doi:10.1109/TGRS.2010.2091416.~~https://doi.org/10.1109/TGRS.2010.2091416.

Rodgers, C. D., 2000: Inverse Methods for Atmospheric Sounding: Theory and Practice. *Series on Atmospheric, Oceanic and Planetary Physics*, Vol. 2, World Scientific, 238 pp.

~~Rose, T., S. Crewell, U. Löhnert, C. Simmer, 2005: A network suitable microwave radiometer for operational monitoring of the cloudy atmosphere, *Atmospheric Research*, **75**, Issue 3, 183–200, https://doi.org/10.1016/j.atmosres.2004.12.005.~~

Rosenkranz, P. W., 1998: Water vapour microwave continuum absorption: A comparison of measurements and models. *Radio Science*, **33**, 919–928~~.~~, https://doi.org/10.1029/98RS01182.

Shaw, W., and Coauthors, 2019: The Second Wind Forecast Improvement Project (WFIP 2): General Overview. *Bull. Am. Meteor. Soc.*, **100(9)**, 1687–1699, https://doi.org/10.1175/BAMS-D-18-0036.1.

Formatted: *Space After: 12 pt, Border: Top: (No border), Bottom: (No border), Left: (No border), Right: (No border), Between : (No border)*

Formatted: *Space After: 12 pt, Line spacing: Double, Border: Top: (No border), Bottom: (No border), Left: (No border), Right: (No border), Between : (No border)*

Solheim, F., J. R. Godwin, J., and R. Ware, 1998a: Passive ground-based remote sensing of atmospheric temperature, water vapor, and cloud liquid profiles by a frequency synthesized microwave radiometer. *Meteorol. Z.*, **7**, 370–376.

Solheim F., J. R. Godwin, E. R. Westwater, Y. Han, S. J. Keihm, K. Marsh, R. Ware, 1998b: Radiometric profiling of temperature, water vapor and cloud liquid water using various inversion methods. *Radio Science*, **33**, 393–404, https://doi.org/10.1029/97RS03656.

Stankov, B. B., E. R. Westwater, and E. E. Gossard, 1996: Use of wind profiler estimates of significant moisture gradients to improve humidity profile retrieval. *J. Atmos. Oceanic Tech.*, **13**, 1285-1290~~.~~, DOI: https://doi.org/10.1175/1520-0426(1996)013<1285:UOWPEO>2.0.CO;2.

Strauch, R. G. , D. A. Merritt, K. P. Moran, K. B. Earnshaw, and D. V. De Kamp, 1983: The Colorado wind-profiling network. *J. Atmos. Oceanic Technol.*, **1**, 37–49, https://doi.org/10.1175/1520-0426(1984)001<0037:tcwpn>2.0.co;2.

Turner, D. D., and U. Löhnert, 2014: Information content and uncertainties in thermodynamic profiles and liquid cloud properties retrieved from the ground-based Atmospheric Emitted Radiance Interferometer (AERI). *J. Appl. Meteor. Clim.*, **53**, 752–771, https://doi.org/10.1175/JAMC-D-13-0126.1.

Turner, D. D., and W. G. Blumberg, 2019: Improvements to the AERIoe thermodynamic profile retrieval algorithm. *IEEE Journal of Selected Topics in Applied Earth Observations and Remote Sensing*, **12(5)**, 1339–1354, https://doi.org/10.1109/JSTARS.2018.2874968.

Formatted: *Space After: 12 pt, Line spacing: Double, Border: Top: (No border), Bottom: (No border), Left: (No border), Right: (No border), Between : (No border)*

Turner, D. D., and U. Löhnert, 2020: Ground-based Temperature and Humidity Profiling: Combining Active and Passive Remote Sensors. *In revision to Atmos. Meas. Tech.* ~~*Discuss.*, https://doi.org/10.5194/amt-2020-352~~*Discuss.*, https://doi.org/10.5194/amt-2020-352.

Ware R., Solheim F., Carpenter R., and Coauthors, 2003: A multi-channel radiometric profiler of temperature, humidity and cloud liquid. *Radio Science*, **38**, No. 4, 8079, https://doi.org/10.1029/2002RS002856.

Weber, B. L~~.,~~., D. B. Wuertz, D. C. Welsh, and R. Mcpeek, ~~1992~~1993: Quality controls for profiler measurements of winds and RASS temperatures. *J. Atmos. Oceanic Technol.*, **10**, 452–464, https://doi.org/10.1175/1520-0426(1993)010<0452:qcfpmo>2.0.co;2

Wilczak, J. M., and Coauthors, 2019: The Second Wind Forecast Improvement Project (WFIP2): Observational Field Campaign. *Bull. Am. Meteor. Soc.*, **100(9)**, 1701–1723, https://doi.org/10.1175/BAMS-D-18-0035.1.

Wolfe, D. E. and R. J. Lataitis, 2018: Boulder Atmospheric Observatory: 1977–2016: The end of an era and lessons learned. *Bull. Am. Meteor. Soc.*, **99**, 1345–1358, https://doi.org/10.1175/BAMS-D-17-0054.1.

Formatted: *Space After: 12 pt, Line spacing: Double, Border: Top: (No border), Bottom: (No border), Left: (No border), Right: (No border), Between : (No border)*